sustainability

MDPI

Article

Thermodynamic Performance Assessment of Standalone Liquid Air Energy Storage Systems With and Without Organic Rankine Cycle Integration for Sustainable Energy Storage Applications

Muhsin Kılıç [1,*] and Fatih Özcan [2]

[1] Department of Mechanical Engineering, Bursa Uludağ University, Görükle, Bursa 16059, Türkiye
[2] Department of Machinery and Metal Technologies, Orhangazi Yeniköy Asil Çelik Vocational School, Bursa Uludağ University, Bursa 16800, Türkiye; fatihozcan@uludag.edu.tr
* Correspondence: mkilic@uludag.edu.tr

Abstract

This study presents a comprehensive exergy-based thermodynamic analysis of a standalone liquid air energy storage (LAES) system integrated with internal thermal storage and an Organic Rankine Cycle (ORC) for sustainable large-scale energy storage applications. Unlike conventional studies, this work focuses on providing a scalable design framework by quantifying storage fluid requirements on a per-unit-mass-flow and per-MWh-capacity basis, enabling the results to be generalized for various power outputs and storage capacities. The proposed system configurations with two- and three-stage compression were compared in terms of liquid yield, round-trip efficiency (RTE), exergy efficiency, and storage fluid requirements. Results indicate that the optimal operating pressures are 190 bar for charging and 130 bar for discharging. At 200 bar charging pressure, the liquid yield increases from 0.51 (at 60 bar) to 0.86, while the maximum RTE reaches 62% in the base case and 68% with ORC integration. Incorporating ORC enhances the RTE by approximately 6–7% compared with conventional configurations through improved low-grade waste heat recovery and energy utilization. The two-stage compression configuration with ORC demonstrates the best thermodynamic performance, providing higher exergy efficiency, greater net power output, and lower thermal storage requirements. Furthermore, the reduction in thermal storage fluid demand contributes to improved resource utilization and lower infrastructure requirements for large-scale deployment. Additional sensitivity analyses indicate that thermal losses significantly reduce system performance, whereas ambient temperature fluctuations within ±15 K have only a minor influence on round-trip efficiency and liquid yield due to compensating effects between charging and discharging processes. The findings of this study provide scalable design insights for LAES systems and demonstrate the potential of ORC-assisted LAES technology to support renewable energy integration, sustainable grid flexibility, and low-carbon energy infrastructure development.

Keywords: liquid air energy storage (LAES); cryogenic energy storage; exergy analysis; organic rankine cycle (ORC); sustainable energy storage; low-carbon energy storage

Check for updates

Academic Editor: Andrea Nicolini

Received: 18 April 2026
Revised: 20 May 2026
Accepted: 25 May 2026
Published: 27 May 2026

Copyright: © 2026 by the authors. Licensee MDPI, Basel, Switzerland. This article is an open access article distributed under the terms and conditions of the Creative Commons Attribution (CC BY) license.

1. Introduction

The increasing share of renewable energy in global electricity supply is a cornerstone of strategies for mitigating climate change, yet the variability of solar and wind generation presents major obstacles to grid stability [1]. Power systems will face operational risks due to renewable energy's irregular and intermittent nature, such as problems with

frequency and voltage stability [2,3]. Energy storage technologies are indispensable for overcoming these challenges, enabling peak shaving, frequency regulation, and large-scale integration of renewables [3,4]. Large-scale energy storage technologies are considered critical enablers for sustainable power systems because they support renewable energy penetration, reduce curtailment losses, improve grid flexibility, and facilitate low-carbon energy transitions. Recent research further confirms that thermal energy storage systems exhibit unique engineering applicability in grid frequency regulation and renewable energy grid integration, especially in countries advancing energy transition, where they have entered the demonstration application stage [5]. Energy storage systems can accumulate energy during off-peak times and discharge it at peak demand, facilitating the integrated utilization of renewable energy and the electrical grid [6]. As the demand for clean energy continues to surge, the integration of energy storage solutions becomes increasingly vital. These systems allow for the seamless balancing of supply and demand, acting as a buffer between intermittent renewable sources such as solar and wind and the grid's energy requirements. By storing excess energy generated during peak production periods and discharging it when demand peaks, energy storage not only enhances the reliability of power systems but also maximizes the utilization of renewable resources, thereby minimizing reliance on fossil fuels. The Energy Storage System (ESS) utilized in the electricity grid is typically autonomously regulated, operating in three modes: charging, storage, and discharging. It can retain energy produced in the power system and subsequently send the stored energy back to the power system when required. Moreover, advancements in storage technologies—ranging from lithium-ion batteries to pumped hydro and beyond—are driving innovations that can lower costs and increase efficiency. This technological evolution is essential for overcoming the traditional barriers associated with renewable energy, such as variability and unpredictability. Finally, effective energy storage solutions can empower utilities and consumers alike, enabling a transition to decentralized energy models where local storage systems complement grid operations. This decentralized approach not only supports energy resilience but also fosters community engagement and energy autonomy, further accelerating the shift towards sustainable energy futures. Owing to the vast potential of energy storage and the rising development of the market, considerable research efforts have been made to provide a complete study and review on the types, applications, and evaluation systems of energy storage systems [1,2,6,7].

Among the established storage options, pumped hydro energy storage (PHES) and compressed air energy storage (CAES) are widely deployed, but remain limited by geographical requirements [8–15]. Electrochemical batteries, particularly lithium-ion systems, offer high round-trip efficiencies but face concerns related to cost, material scarcity, recycling, and lifetime [16–18]. These constraints have stimulated interest in alternative large-scale technologies such as Liquid Air Energy Storage (LAES) [14]. LAES systems with the required high energy capacity and power can be installed anywhere [19,20].

LAES is increasingly recognized as a competitive thermo-mechanical energy storage option due to its high energy density, scalability, and minimal geographic limitations [10,14,21,22]. Unlike CAES, LAES systems can store liquefied air at near-atmospheric pressure in insulated cryogenic tanks, eliminating the need for underground caverns [11,23]. Moreover, the technology is compatible with industrial heat sources and LNG regasification terminals, which can further enhance performance [24–29].

An LAES system, as shown in Figure 1, typically involves three stages: charging, storage, and discharging. During charging, multi-stage compression and liquefaction processes generate high-grade heat, which can be stored in hot reservoirs, while the high-pressure air is cooled down to ambient temperatures [30]. After compression and cooling, high-pressure air is further cooled to cryogenic temperatures utilizing cold storage [31].

Then, high-pressure cooled air is expanded to atmospheric pressure using a cryogenic expander. After that, the liquid air is separated from any remaining gas using a separator, and the liquefied air is taken into the liquid air storage tank [30,32]. During discharging, liquid air is pumped, evaporated, reheated, and expanded through turbines to generate electricity, while cold energy is recovered through cryogenic thermal storage [33,34]. During the evaporation process, cold energy is produced and stored utilizing the cold storage assemblies at low (down to 93 K) and warm (down to 214 K) temperatures. This internally stored cold energy can be used to support air liquefaction [35]. Meanwhile, the heat from the hot storage can be used as the high-temperature source during reheating in the discharging process [36]. Despite its potential, the round-trip efficiency (RTE) of LAES typically remains in the range of 50–60%, which is lower than that of batteries and PHES [21,37].

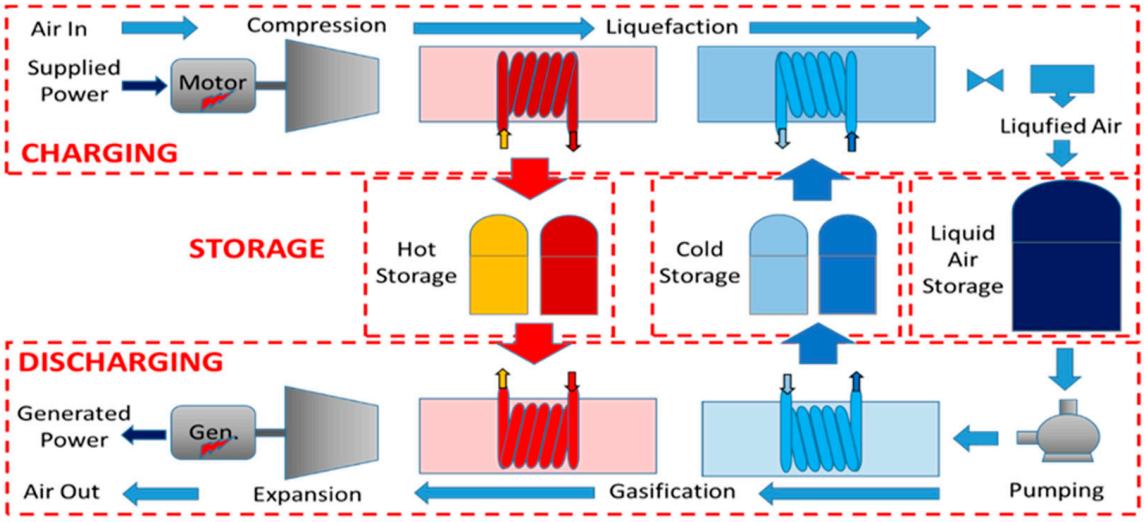


Figure 1. Schematics of the overall system configuration of cryogenics-based energy storage show the pathway of process fluid and energy flow.

Various strategies have been explored to enhance LAES performance [22]. Researchers have investigated advanced liquefaction cycles [11,38,39], packed-bed thermal storage [40–42], and hybridization with renewable sources [43–46]. In particular, the integration of Organic Rankine Cycles (ORCs) has emerged as an effective approach to utilize low-grade compression heat for additional power generation [47–49]. Hybrid LAES–ORC systems improve energy and exergy efficiencies and reduce the required volumes of hot and cold storage [21,34].

Despite these advances, important research gaps persist. First, many studies adopt case-specific models that limit the scalability of their conclusions [2,21,37]. Second, the role of thermal storage requirements is often oversimplified, despite their critical influence on efficiency and cost [24,39]. Third, the combined influence of compression stage number, charging/discharging pressures, and ORC integration has not been systematically investigated.

To address these gaps, the main contributions of this study can be summarized as follows. This study presents a generalized exergy-based thermodynamic analysis of LAES systems both with and without ORC integration. Unlike prior work, the results are expressed per unit mass flow of air, enabling scalability across different storage capacities and power outputs. Two-stage and three-stage compression configurations are comparatively investigated. By systematically varying design parameters, this study quantifies their impact on liquid yield, round-trip efficiency, exergy efficiency, and storage-fluid requirements. The influence of charging and discharging pressures on thermal storage requirements is quantified in detail. This paper presents practical insights on sizing hot

and cold thermal storage for large-scale LAES deployment. The findings provide not only performance benchmarks but also practical design guidelines for future LAES systems and contribute to the development of sustainable large-scale energy storage technologies, thereby strengthening the optimum case for large-scale adoption of sustainable cryogenic energy storage.

2. System Layout

The layout of the present LAES system with two-stage compression is given in Figure 2, and three-stage compression is shown in Figure 3. Default parameters considered for the modeling are given in Table 1. In this configuration, air is compressed in a two-stage inter-cooled process. The compression waste heat is stored by using thermal oil. After the compression stage, compressed air is cooled by the returning air from the separator, and the liquefied air is stored in the storage tank.

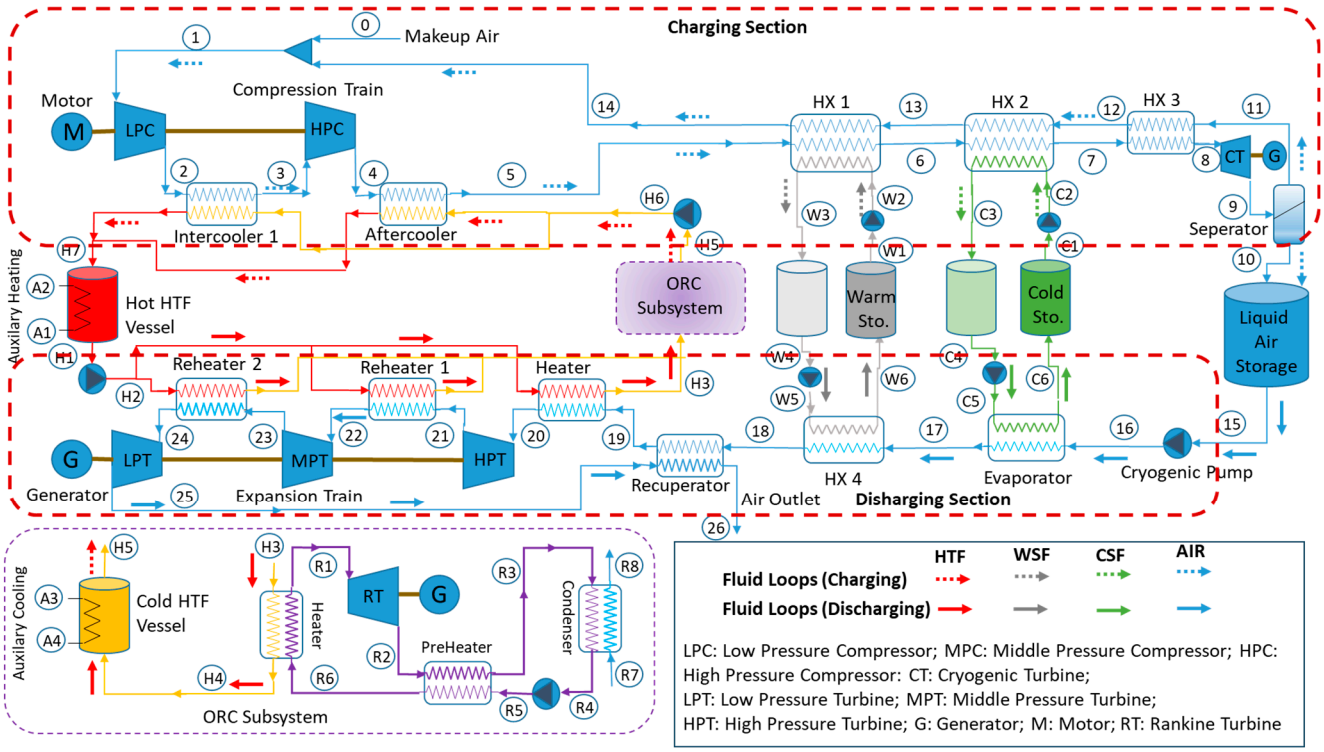


Figure 2. Schematics of the present LAES system with two compression stages.

Propane and methanol are considered for the cold storage section. In the cold storage section, the liquefied air's cold exergy is stored for reuse later to liquefy it at high efficiency. The expansion process is a three-stage process with interheating between stages. Thermal oil from the hot storage is used for interheating. Thermal oil coming from the hot storage section splits into three branches: Reheater2, Reheater1, and Pre-heater. A recuperator is used for the heat recovery of the air exiting the superheater and the air at the lower-pressure turbine outlet. A new configuration is recommended to enhance the system's efficiency. In the proposed configuration, the waste heat of the thermal oil is recovered by the ORC with the aim of increasing power production. In addition, a heat exchanger, HX3, is placed after HX2 to improve the system performance.

An evaporator (heater), turbine (expander), condenser, pump, and an internal heat exchanger known as a pre-heater are the five parts of the ORC subsystem [50,51]. The heat required to operate the ORC subsystem is provided by the waste heat of the thermal

oil through H3 to H4. Heat is transferred to the working fluid circulating in the ORC subsystem by thermal oil entering the heater.

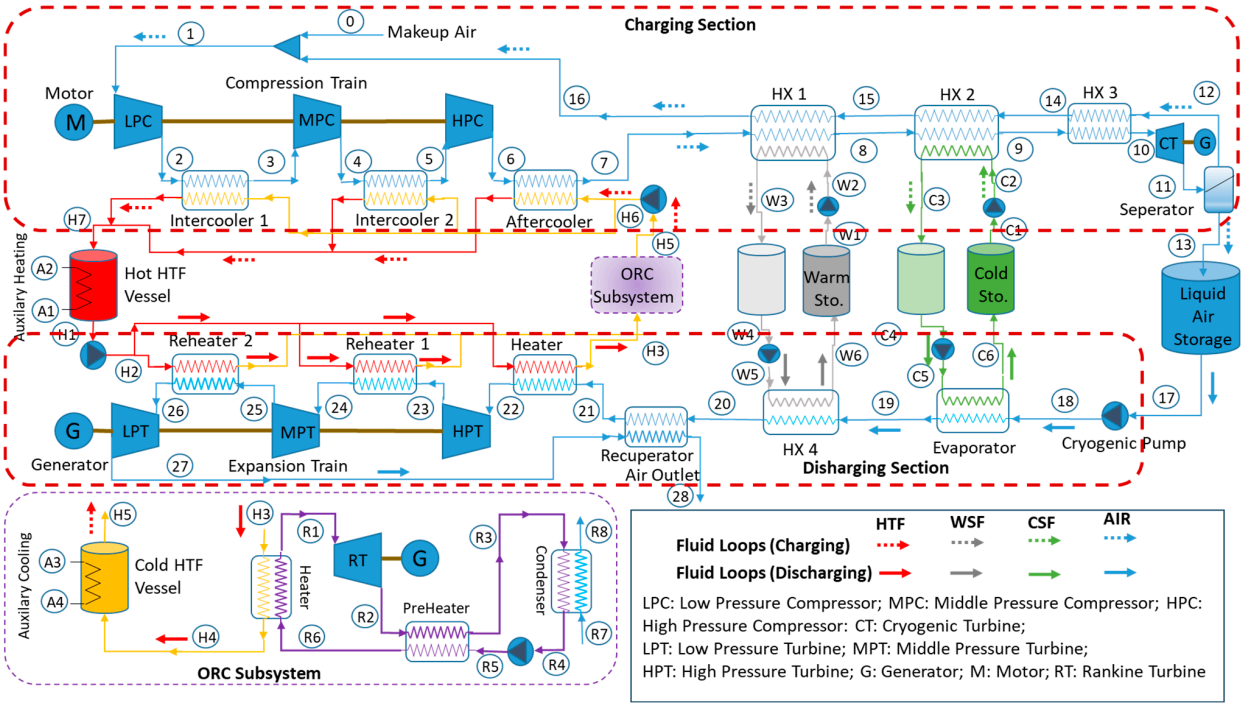


Figure 3. Schematics of the present LAES system with three compression stages.

The working fluid expands to the condenser pressure after entering the expander at the evaporation pressure. Supercooling occurs in the condenser when the working fluid transfers its heat to the cooling fluid at constant pressure, causing it to condense fully. After passing through the pump and being compressed, the fluid exiting the condenser reaches the heater's evaporation pressure. By using a pre-heater, an internal heat recovery process is achieved. The low-temperature liquid-phase organic fluid from the pump receives heat from the high-temperature vapor-phase organic fluid exiting the turbine in the pre-heater. Superheating happens when the working fluid enters the heater and uses the thermal oil's waste heat to entirely evaporate. Table 1 provides the characteristics of some frequently employed refrigerants in the ORC systems. Among them, R1233zd(E) was selected as the working fluid in the ORC subsystem. R1233zd(E) was selected because of its environmentally friendly characteristics, low global warming potential, negligible ozone depletion potential, safety characteristics, and suitability for ORC applications [52–55]. The thermophysical properties of R1233zd(E) remain stable under moderate partial-load conditions because of its favorable saturation characteristics and thermal stability [55,56]. Compared with R245fa and R600, R1233zd(E) provides improved environmental performance, safety, and stable operation under moderate evaporation temperatures commonly encountered in LAES waste heat recovery systems [55,56].

Table 1. Characteristics of some working fluids used in ORC systems.

Fluid	Critical Temp. (K)	GWP	ODP	Safety	Suitability	Ref.
R1233zd(E)	439	1	~0	Safe	Excellent	[55]
R245fa	427	1030	0	Moderate	Good	[54,55]
R600	408	4	0	Flammable	Moderate	[54,55]
R123	457	77	~0	Moderate	Good	[54]

3. Methodology

This section presents the governing equations utilized in the model and the model's validation.

3.1. Numerical Model

In this section, governing equations of thermodynamic analysis are presented. The main assumptions considered for the calculations are presented below.

- The studied system operates in a steady-state condition for both the charging and discharging processes, i.e., they operate separately.
- The potential and kinetic energy variations are neglected.
- Hot and cold storage are isolated adiabatically, so there is no heat transfer to the environment.
- Auxiliary pump losses in the hot and cold storages are neglected in the model.
- An equal pressure ratio is taken for the compressor stages during the charging process.
- An equal pressure ratio is taken for the expansion stages during the discharging process.
- The inlet mass flow rate of the air for both charging and discharging processes is 1 kg/s.
- Default parameters used in the model are given in Table 2.

Table 2. Default parameters of the LAES.

Parameter	Value	Unit
Ambient temperature	298	K
Ambient pressure	101	kPa
Minimum propane temperature	95	K
Minimum methanol temperature	214	K
Cooling water temperature	293	K
Pinch point of heaters	10	K
Pinch point of intercoolers	10	K
Pinch point of cold box heat exchangers	5	K
The pinch point of the evaporator	5	K
Relative pressure drops of heat exchangers	1	%
Heat exchanger efficiency	85	%
Efficiency of intercooler, pre-heater, heater, reheater	85	%
The isentropic efficiency of the compressor	85	%
The isentropic efficiency of the turbine	85	%
The isentropic efficiency of the cryo-turbine	70	%
The isentropic efficiency of the cryo-pump	70	%
Superheating in ORC heater	5	K
Subcooling in ORC evaporator	5	K

For energy analysis, the energy and mass conservation equations are essential. The mass balance equation is given below:

$$\sum \dot{m}_{in} = \sum \dot{m}_{out} \tag{1}$$

where $\dot{m}$ is the mass flow rate.

Energy and exergy rate equations for any system can be given as:

$$\sum \dot{m}_{in} h_{in} + \dot{Q}_{cv} - \sum \dot{m}_{out} h_{out} - W_{cv} = 0 \tag{2}$$

$$\sum \dot{E}x_{in} - \sum \dot{E}x_{out} + \sum \dot{E}x_{heat} + \sum \dot{W} - \dot{E}x_{destruction} = 0 \tag{3}$$

In Equation (3), the exergy term $\dot{E}x$ is the sum of physical and chemical energies. The following equation can express physical exergy:

$$\dot{E}x = \dot{m}[(h - h_0) - T_0(s - s_0)] \quad (4)$$

where s is the specific entropy.

$$\dot{E}x_{heat} = Q\left(1 - \frac{T_0}{T_i}\right) \quad (5)$$

The isentropic efficiency of the compressors can be calculated as follows:

$$\eta_{comp} = \frac{h_{out,s} - h_{in}}{h_{out} - h_{in}} \quad (6)$$

The pressure ratio of the air compressors can be calculated as follows:

$$PR = \frac{P_{out,comp}}{P_{in,comp}} \quad (7)$$

The power consumption of each compressor, $\dot{W}_{comp,i}$, and the total power requirement for compression, $\dot{W}_{comp,tot}$, are given as:

$$\dot{W}_{comp,i} = \dot{m}_{a,i}(h_{i,out} - h_{i,in}) \quad (8)$$

$$\dot{W}_{comp,tot} = \sum_{i=1}^{n} \dot{W}_{comp,i} \quad (9)$$

The power output of each turbine, $\dot{W}_{tr,i}$, and the total power output from expansion, $\dot{W}_{tr,tot}$, are given as:

$$\dot{W}_{tr,i} = \dot{m}_{a,i}(h_{i,out} - h_{i,in}) \quad (10)$$

$$\dot{W}_{tr,tot} = \sum_{i=1}^{n} \dot{W}_{tr,i} \quad (11)$$

The power consumption of cryo-pump, $\dot{W}_{p,cryo}$, in the discharging section of the LAES, is given as:

$$\dot{W}_{p,cryo} = \dot{m}_a(h_{out} - h_{in}) \quad (12)$$

$\dot{W}_{net,ch}$ is the net power consumption in the charging process, which can be found below:

$$\dot{W}_{net,ch} = \dot{W}_{comp,tot} - \dot{W}_{tr,cryo} \quad (13)$$

where $\dot{W}_{tr,cryo}$ is the power generated by the cryo-turbine in the charging section of the LAES system.

$\dot{W}_{net,dis}$ is the net power output from the discharging process, which can be found below:

$$\dot{W}_{net,dis} = \dot{W}_{tr,tot} - \dot{W}_{p,cryo} \quad (14)$$

When the ORC subsystem is integrated into the LAES system, as shown in Figures 2 and 3. The power produced by the ORC turbine can be calculated as follows:

$$\dot{W}_{tr,ORC} = \dot{m}_{wf,ORC}(h_{R1} - h_{R2}) \quad (15)$$

The power consumption of the pump in the ORC subsystem, $\dot{W}_{p,ORC}$, is given as:

$$\dot{W}_{p,ORC} = \dot{m}_{wf}(h_{R5} - h_{R4}) \quad (16)$$

The net power output from the ORC subsystem, $\dot{W}_{net,ORC}$, can be found below:

$$\dot{W}_{net,ORC} = \dot{W}_{tr,ORC} - \dot{W}_{p,ORC} \tag{17}$$

The net power output, $\dot{W}_{net,dis}$, from the discharging process of the LAES system with the ORC subsystem can be found below:

$$\dot{W}_{net,dis} = \dot{W}_{tr,tot} - \dot{W}_{p,cryo} + \dot{W}_{net,ORC} \tag{18}$$

Performance Parameters

Only a fraction of the air can be liquefied for the real liquefaction systems. The liquid yield, y, can be expressed as the ratio of the mass flow rate of the produced liquid air ($\dot{m}_{lq}$) to the mass flow rate of the compressed air ($\dot{m}_a$) in the system. The liquid yield is an essential performance parameter in any plant involving air liquefaction. Liquid yield can be presented as follows:

$$y = \frac{\dot{m}_{lq}}{\dot{m}_a} \tag{19}$$

The overall performance of the LAES system can be evaluated using the round-trip efficiency (RTE). The RTE is defined as the ratio of the net work output during the discharging process to the net work input during the charging process, both normalized by the flow rate of liquefied air. It should be emphasized that, during the charging process, the inlet air mass flow rate is taken as unity; however, only a fraction of the compressed air is liquefied, corresponding to the liquid yield value (y). Consequently, additional work is required to produce a unit mass flow rate for liquefied air. Therefore, for the same inlet air mass flow rate, the charging and discharging durations are not identical, and the stored liquid air is depleted within a shorter duration during the discharging process in proportion to the liquid yield value. Under the present steady-state formulation, this effect is inherently accounted for through normalization with respect to the liquefied air mass flow rate. Therefore, the round-trip efficiency, RTE, can be calculated as follows:

$$RTE = y\frac{\dot{W}_{net,dis}}{\dot{W}_{net,ch}} \tag{20}$$

In this study, all the computations are performed based on the unit mass of air used in the system. Meanwhile, a portion of this air mass (known as yield value, y) is liquefied during the charging procedures. Therefore, a relation could be derived to calculate the mass flow rates of the storage fluids (propane, methanol, and hot storage fluid) in the charging and discharging process.

$$\dot{m}_{sf,ch} = y \cdot \dot{m}_{sf,dis} \tag{21}$$

where $\dot{m}_{sf,dis}$ (kg/s) is the mass flow rate of any storage fluid (either propane, methanol, or hot storage fluid) in the discharging process; $\dot{m}_{sf,ch}$ (kg/s) is the mass flow rate of any storage fluid (either propane, methanol, or hot storage fluid) in the charging process.

Charging section exergy efficiency, $\eta_{Ex,ch}$, can be calculated as follows:

$$\eta_{Ex,ch} = \frac{\dot{E}x_{HS,ch} + \dot{E}x_{la,ch}}{\dot{W}_{net,ch} + \dot{E}x_{CS,ch}} \tag{22}$$

where $\dot{E}x_{HS,ch}$ is the stored exergy flow rate on the hot storage during the charging process, $\dot{E}x_{la,ch}$ is the stored exergy flow rate on the liquid air storage during the charging process, $\dot{E}x_{CS,ch}$ is the recovered exergy flow rate from the cold storage during the charging process.

Discharging section exergy efficiency, $\eta_{Ex,dis}$, can be calculated as follows:

$$\eta_{Ex,dis} = \frac{\dot{W}_{net,dis} + \dot{E}x_{CS,dis}}{\dot{E}x_{HS,dis} + \dot{E}x_{la,dis}} \quad (23)$$

where $\dot{E}x_{CS,dis}$ is the stored exergy flow rate on the cold storage during the discharging process, $\dot{E}x_{la,dis}$ is the recovered exergy flow rate from the liquid air storage during the discharging process, $\dot{E}x_{HS,ch}$ is the recovered exergy flow rate from the hot storage during the discharging process.

The mathematical model code for the LAES systems is prepared by using the Engineering Equation Solver (EES, Version 12) [57], and the set of equations in the model is iteratively solved by means of the EES software. In the calculations, the EES internal real fluid property libraries are employed to calculate the fluid properties.

3.2. Validation

The present mathematical model code is validated by comparing the results with those of similar studies in the literature. The model code of the LAES system is validated by using the data presented by Guizzi et al. [30]. The LAES system was modified as given in the study of Guizzi et al. [30]. Then, the operating conditions of the LAES system were taken as defined in the reference work. According to the reference work, the discharge (gasification section) pressure was taken as 6.5 MPa. The charging (liquefaction section) pressure is varied between 10 and 20 MPa, and the influence on the liquid yield and the round-trip efficiency is calculated with the present simulation model. Figure 4 shows the comparisons between the present calculation results and the data reported in the reference study. The simulation results for the defined operating conditions show that both the liquid yield and the round-trip efficiency increase until a maximum is reached. After that, the liquid yield stays constant, and the round-trip efficiency starts to decrease. The results of the present study are in good agreement with those of Guizzi et al. [30]. Meanwhile, the maximum deviation remained within 3.2%, confirming the reliability of the developed thermodynamic model for future calculations.

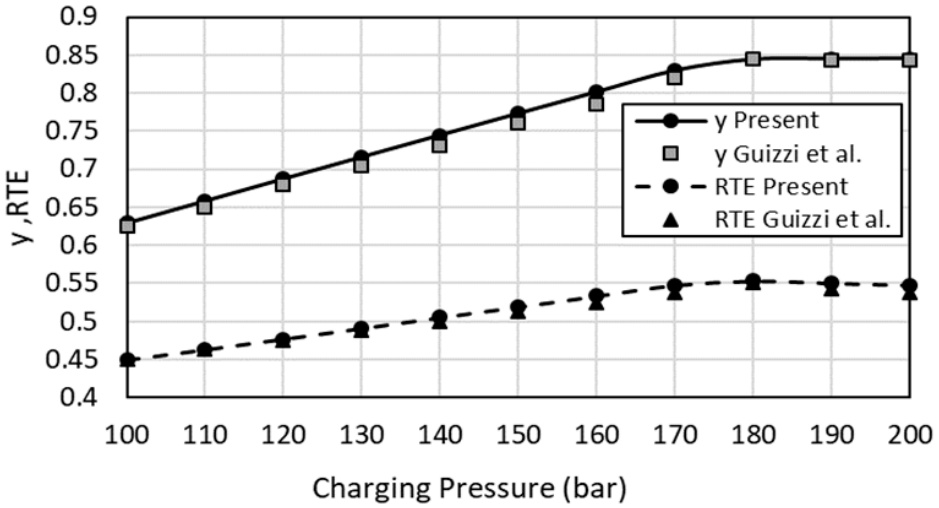


Figure 4. Mathematical model validation with Guizzi et al. [30].

4. Results and Discussion

This section comprises four subsections: Energy analysis, Exergy analysis, Sustainability Implications, and General discussions.

4.1. Energy Analysis

Apart from the previous studies in the current literature, it is noticed that the hot and cold storage mass flow rates depend on the operating conditions of the LAES system. Cold storage (cold (propane) and warm (methanol) storage) mass flow rates depend on the discharge process operating pressures. On the other hand, the hot storage mass flow rate and the storage temperature depend on the charging process operating pressure. Meanwhile, the liquid yield value affects both the charging and discharging times, as well as the mass flow rates of the storage fluids. For the unit air mass flow rate, the calculation procedure of the mass flow rates of the storage fluids can be ordered as follows:

(i) Calculate the low-temperature (propane) and warm-temperature (methanol) mass rates of cold storage fluids for different discharge process pressures.
(ii) Using cold storage mass flow rates (obtained from the discharge process) for the given discharge process pressure, multiplied by the liquid yield, calculate the liquid yield values for different charge process pressures (note that this step can be realized iteratively).
(iii) Calculate the required hot storage fluid mass flow rates to cool down the compressed air at the intercoolers and the after-cooler for the different charge process pressures.
(iv) Calculate the hot storage fluid temperature recovered from the compressed air at the intercoolers and the after-cooler for the different charge process pressures.
(v) Using the hot storage fluid mass flow rates and the liquid yield value (obtained from the charging process) for the given charge process pressure, calculate the hot storage fluid mass flow rate to heat the compressed air at the heaters for the different discharge process pressures.

It is essential to highlight that all calculations were made based on the unit air mass flow rate. Therefore, energy storage capacity and power output are found based on the unit air mass flow rate. The study results can be easily applied to systems with greater power output and energy storage capacity by increasing the air mass flow rate.

The effect of the discharge pressure on the mass flow rate ratio (the ratio of the refrigerant mass flow rate to the liquefied air) of cold and warm storage is given in Figure 5. Results show that as the discharge pressure increases, a higher share of methanol is required. In contrast, a lower share of propane is needed as the discharge pressure increases. The mass flow rate ratio of propane is much higher than the mass flow rate of methanol at all discharge pressures.

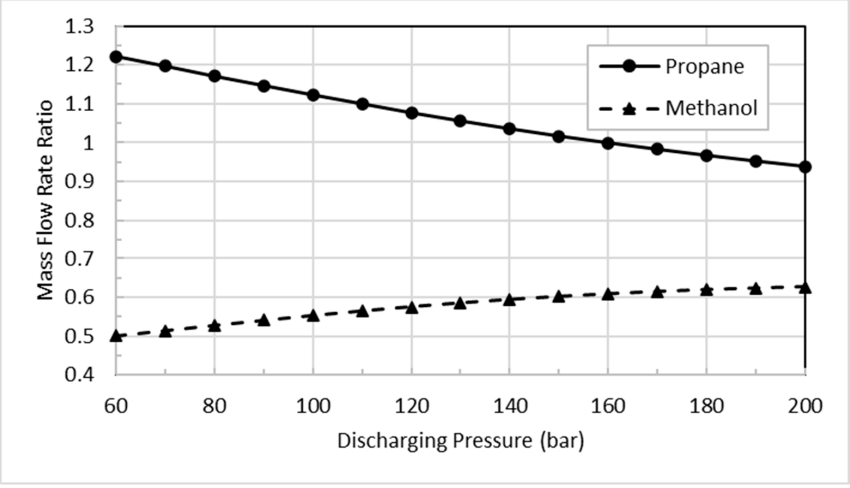


Figure 5. Variation of the cold (propane) and warm (methanol) storage mass flow rate ratios ($m_{rf.dis}/m_{a,dis}$) with the discharging pressure.

It is essential to highlight that one of the most substantial design parameters is selecting the compression and expansion stage numbers. Most literature data discuss the charge and discharge sections separately; however, the discharge section is affected by the charging section if there is thermal recovery between them [13]. Similarly, the charge section is influenced by the discharge section. In this part, the number of compression stages was varied from 2 to 3. The expansion stage number is 3 for both cases. Thermal oil is selected to transfer the compression heat from the charging section to the discharging section. The temperature of the thermal oil changes based on the number of compression stages, and it influences the air temperature at the turbine inlet and the power production. Figure 6 shows the temperature variation of the thermal oil in the hot storage section at different charging pressures. Results were given for both two-stage and three-stage compression configurations. It can be seen that the temperature of the thermal oil at the hot storage section is much more significant for the system with 2-stage compression compared to the system with 3-stage compression. At 180 bar, the temperature of the hot storage inlet (H7) is 671 K for the system with 2-stage compression and 514.8 K for 3-stage compression. Therefore, for two-stage compression, the expansion section can take advantage of high-grade thermal energy. The results will be further evaluated regarding the second law of thermodynamics. For both systems, increasing the charging pressure increases the hot storage temperature.

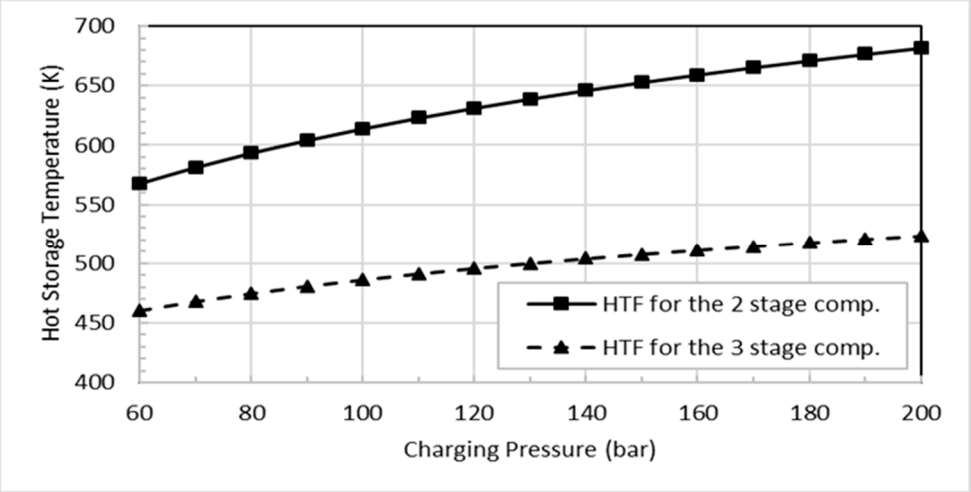


Figure 6. Variation of the hot storage temperature with the charging pressure.

In Figure 7, the influence of the charging pressure on the hot storage mass flow rate ratio is given for charging and discharging sections of the LAES system with 2 and 3 compression stages. It can be seen that the mass flow rate is almost constant for the entire range of the charging pressures. In contrast, the lower charging pressures result in a higher amount of thermal oil mass flow rates during the discharging process because of the lower liquid air yield value at lower charging pressures. As can be seen from the results, a higher charging pressure is required for the discharge section due to higher liquid yield values with increasing charging pressure. In addition, the LAES system with 3 compression stages has a greater amount of thermal oil mass flow rate demand.

This section gives the simulation results for the proposed LAES configuration with two and three compression stages. The reference operating parameters are given in Table 2. The charge and discharge pressures are taken as 18 MPa and 13 MPa, respectively. The stream data for the proposed LAES system with two and three compression stages are presented in Tables 3 and 4. Charging and discharging processes are given separately.

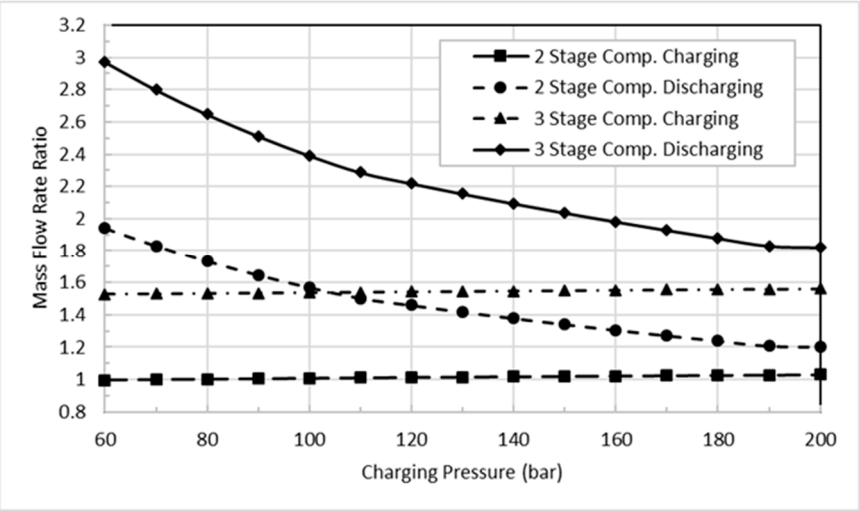


Figure 7. Variation of the hot storage mass flow rate ratio with the charging pressure for 130 bar discharging pressure.

Table 3. Stream data of the LAES configuration for the two compression stages with ORC (for 18 MPa charge and 13 MPa discharge pressures).

Stream No.	m (kg/s)	T (K)	P (MPa)	h (kJ/kg)	s (kJ/kgK)	Fluid
Charging (Liquefaction) Process						
0	0.837	298.1	0.101	298.4	6.86	Air
1	1	298.1	0.101	298.4	6.86	Air
2	1	673.4	1.355	685.3	6.95	Air
3	1	303.2	1.342	300.7	6.13	Air
4	1	688.3	18.00	705.2	6.22	Air
5	1	303.1	17.82	272.3	5.29	Air
6	1	222.8	17.64	161.3	4.87	Air
7	1	100.7	17.46	−73.62	3.34	Air
8	1	99.2	17.29	−76.63	3.33	Air
9	1	78.9	0.101	−92.71	3.40	Air
10	0.837	78.9	0.101	−126.1	2.98	Air
11	0.163	78.9	0.101	78.72	5.54	Air
12	0.163	99.1	0.101	97.15	5.74	Air
13	0.163	209.2	0.101	208.9	6.50	Air
14	0.163	298.1	0.101	298.4	6.86	Air
C2	0.884	93.2	0.101	−181.9	−1.23	Propane
C3	0.884	214.1	0.101	63.4	0.44	Propane
W2	0.49	214.1	0.101	−1353	−4.2	Methanol
W3	0.49	298.1	0.101	−1155	−3.4	Methanol
H6	1.027	298.1	0.101	16.39	0.05	HTF
H7	1.027	671.2	0.101	812.7	1.79	HTF
Discharging (Gasification) Process						
15	1	78.9	0.101	−126.1	2.98	Air
16	1	84.6	13.13	−106.3	3.04	Air
17	1	209.2	12.99	151.6	4.90	Air
18	1	293.2	12.87	267.0	5.37	Air
19	1	435.5	12.74	428.8	5.82	Air
20	1	616.1	12.61	624.7	6.20	Air
21	1	424.5	2.49	423.9	6.29	Air
22	1	624.4	2.47	633.0	6.70	Air
23	1	431.7	0.487	433.0	6.78	Air
24	1	628.2	0.482	637.1	7.17	Air
25	1	440.5	0.101	442.4	7.25	Air
26	1	298.1	0.101	298.4	6.86	Air
C5	1.056	214.1	0.101	62.7	0.44	Propane
C6	1.056	93.2	0.101	−181.5	−1.23	Propane
W5	0.585	298.1	0.101	−1155	−3.4	Methanol
W6	0.585	214.1	0.101	−1353	−4.2	Methanol
H2	1.239	671.2	0.101	812.7	1.79	HTF
H3	1.239	442.6	0.101	324.8	0.90	HTF
H4	1.239	359.2	0.101	146.7	0.45	HTF

Table 4. Stream data of the LAES configuration with three compression stages with ORC (for 18 MPa charge and 13 MPa discharge pressures).

Stream No.	m (kg/s)	T (K)	P (MPa)	h (kJ/kg)	s (kJ/kgK)	Fluid
Charging (Liquefaction) Process						
0	0.837	298.1	0.101	298.4	6.86	Air
1	1	298.1	0.101	298.4	6.86	Air
2	1	520.5	0.572	524.3	6.93	Air
3	1	303.2	0.566	302.4	6.38	Air
4	1	529.8	3.209	533.0	6.45	Air
5	1	303.2	3.177	296.8	5.87	Air
6	1	532.6	18.00	533.9	5.94	Air
7	1	303.2	17.82	272.3	5.30	Air
8	1	222.9	17.64	161.3	4.88	Air
9	1	100.7	17.46	−73.6	3.34	Air
10	1	99.2	17.29	−76.61	3.31	Air
11	1	78.9	0.101	−92.69	3.40	Air
12	0.837	78.9	0.101	−126.1	2.98	Air
13	0.163	78.9	0.101	78.72	5.54	Air
14	0.163	102.4	0.101	97.15	5.78	Air
15	0.163	220.8	0.101	208.9	6.56	Air
16	0.163	298.2	0.101	298.4	6.86	Air
C2	0.884	93.2	0.101	−181.5	−1.23	Propane
C3	0.884	214.1	0.101	62.7	0.44	Propane
W2	0.490	214.1	0.101	−1353	−4.2	Methanol
W3	0.490	298.1	0.101	−1155	−3.4	Methanol
H6	1.556	298.1	0.101	16.39	0.05	HTF
H7	1.556	514.8	0.101	478.8	1.22	HTF
Discharging (Gasification) Process						
17	1	78.9	0.101	−126.1	2.98	Air
18	1	84.6	13.13	−106.3	3.04	Air
19	1	209.2	12.99	151.6	4.90	Air
20	1	293.2	12.87	267.0	5.37	Air
21	1	347.8	12.74	331.3	5.57	Air
22	1	506.4	12.61	505.8	5.99	Air
23	1	345.6	2.49	342.3	6.08	Air
24	1	506.3	2.47	508.7	6.48	Air
25	1	347.5	0.487	347.5	6.56	Air
26	1	506.4	0.482	509.7	6.95	Air
27	1	352.8	0.101	353.5	7.03	Air
28	1	298.1	0.101	298.4	6.86	Air
C5	1.056	214.1	0.101	62.7	0.44	Propane
C6	1.056	93.2	0.101	−181.5	−1.23	Propane
W5	0.585	298.1	0.101	−1155	−3.4	Methanol
W6	0.585	214.1	0.101	−1353	−4.2	Methanol
H2	1.879	514.8	0.101	478.8	1.22	HTF
H3	1.879	388.1	0.101	208.5	0.62	HTF
H4	1.879	340.2	0.101	106.2	0.33	HTF

This section investigates the recommended LAES system with two and three compression stages and three expansion stages at different charging and discharging pressures. The results are given for the system with ORC and without ORC. Charging pressure varies between 60 and 200 bar, and discharging pressure ranges between 100 and 190 bar. The round-trip efficiency of the system is the performance indicator. In Figure 8, the results are given for the base system (without ORC) and the system with ORC. According to the analysis, the optimal pressures of the LAES system are as follows: 130 bar for the discharging process and 190 bar for the charging process. For the system with 2-stage compression, the maximum round-trip efficiency is 62.16% for the base case and 67.65%

for the ORC-included case. The results show that implementing the ORC into the LAES system improves the round-trip efficiency by 8.83%.

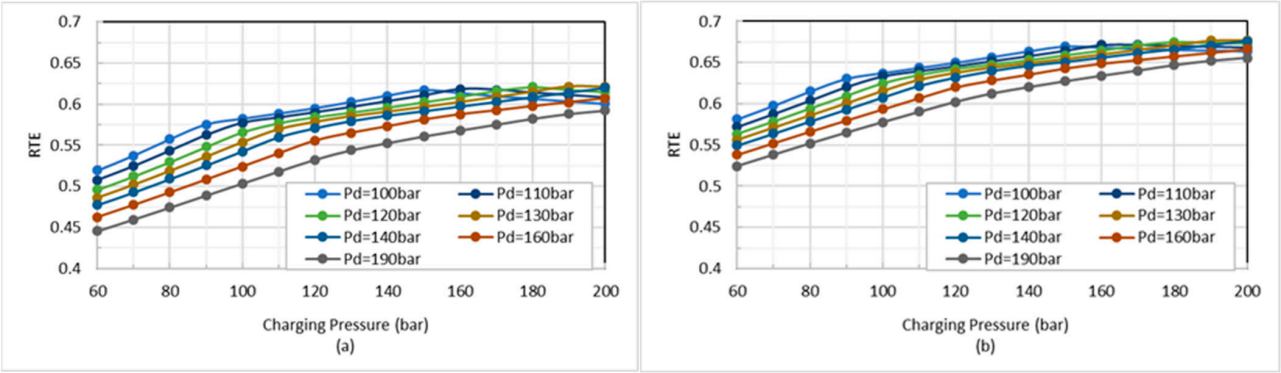


Figure 8. Variation of RTE of the two-stage compression cases with the charging pressure for the different discharging pressures: (**a**) Base one, (**b**) With ORC.

Similar performance improvements through ORC integration have been reported in previous hybrid cryogenic energy storage studies [21,47–49]. However, most previous investigations focused primarily on cycle efficiency enhancement without detailed consideration of scalable thermal storage requirements. In the present study, ORC integration not only improves round-trip efficiency but also contributes to reducing thermal storage fluid demand, which may lower infrastructure requirements and improve the sustainability of large-scale LAES deployment.

Figure 9 presents the results for the 3-stage compression and 3-stage expansion configuration with and without ORC. For this case, 190 bar compression and 130 bar expansion pressure values gave the maximum round-trip efficiency for both cases. The three-stage system with ORC has 61.35%, and without ORC has 57.51% RTE, respectively. For the three-stage system, implementing the ORC subsystem increases the RTE by 6.67%. Generally, the system with 2-stage compression has 8–10% higher round-trip efficiency values than the system with 3 compression stages working at the same operating conditions. As previously shown, the thermal oil temperature is higher for a two-stage configuration. Therefore, the inlet temperature and power output of the turbines are also higher. This results in better round-trip efficiency. Although multi-stage compression generally reduces compressor work through improved intercooling, the present results indicate that excessive staging may reduce the available high-grade thermal energy recovered during compression. Similar thermodynamic trade-offs between compression work reduction and thermal energy quality have also been discussed in advanced LAES studies [22,37]. The higher thermal oil temperature obtained in the two-stage configuration significantly enhances turbine inlet temperatures during discharging, resulting in greater power generation and improved round-trip efficiency.

In Figure 10, the influence of the charging pressure on the liquid yield, the round-trip efficiency, and the net power production is given for two- and three-stage LAES cycles with and without ORC. The amount of the liquefied air highly depends on the charging pressure. The results show that the liquid yield increases as the charging pressure increases for all configurations for a particular value and remains almost constant above that. For all cases, at 60 bar, y is 0.5136, and it increases by 66.8% and becomes 0.856 at 200 bar. The observed increase in liquid yield with charging pressure is consistent with the thermodynamic behavior reported in previous cryogenic liquefaction studies [11,30,38]. Higher charging pressures improve the liquefaction potential of compressed air by increasing the available pressure energy prior to cryogenic expansion. However, beyond approximately 190 bar, the

improvement becomes marginal because of increasing compression work and diminishing gains in liquefaction effectiveness.

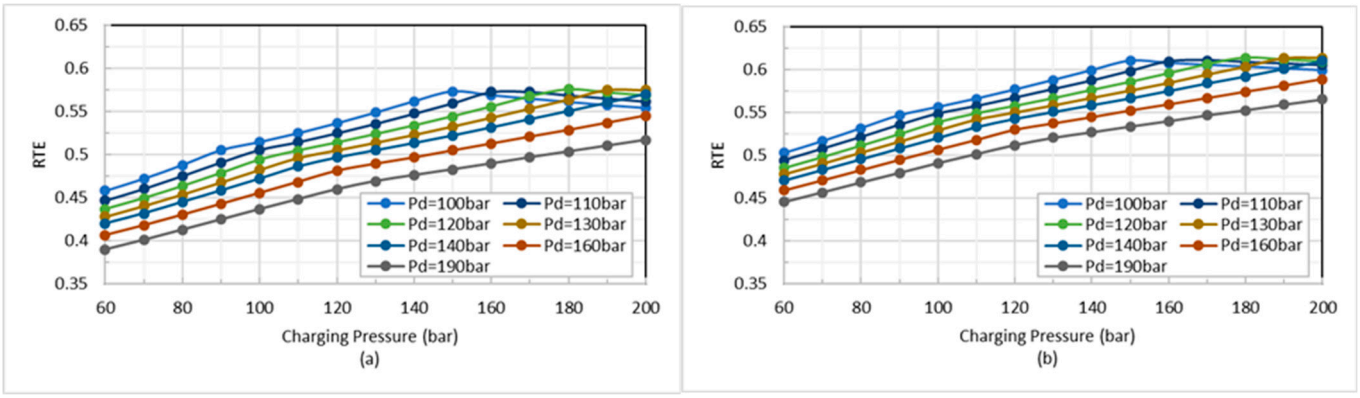
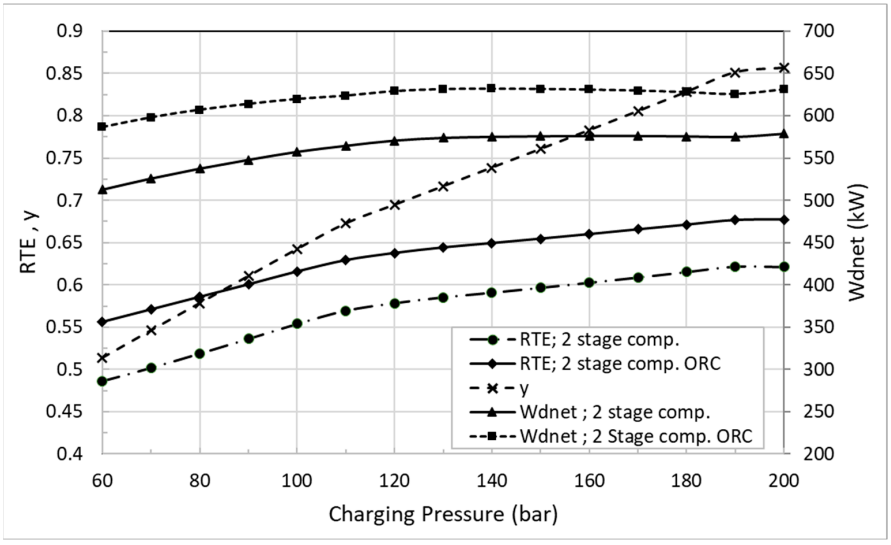
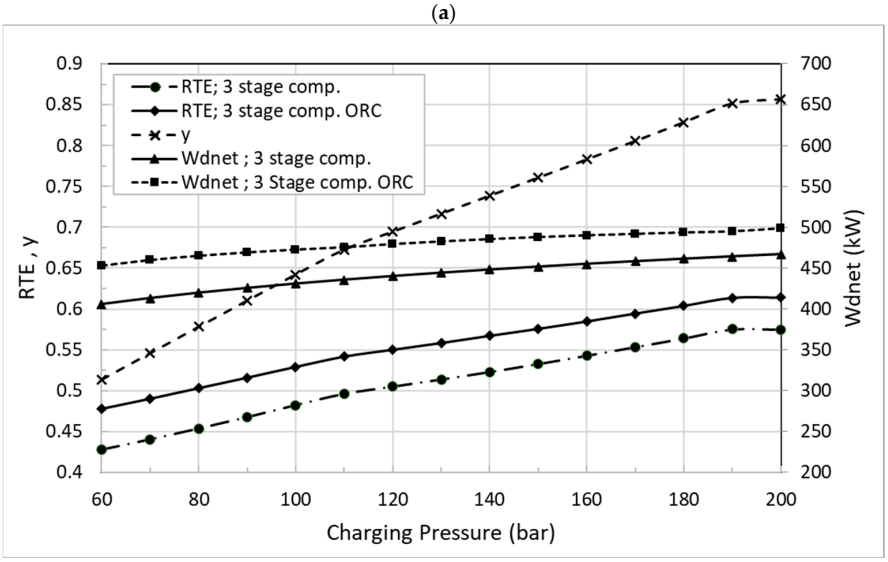


Figure 9. Variation of RTE of the three-stage compression case with the charging pressure for the different discharging pressures: (**a**) Base one, (**b**) With ORC.



(**a**)



(**b**)

Figure 10. Variation of y, RTE, and W_{net} with the charging pressure for the 130 bar discharging pressure: (**a**) 2-stage compression system, (**b**) 3-stage compression system.

Figure 10 also displays the impact of charging pressure on the RTE. As the charging pressure increases, the RTE of the system also increases until 190 bar. Above 190 bar, it remains almost constant. It is also noted that the RTE of the LAES system with two-stage compression and ORC is more significant than other configurations. At 190 bar charging pressure, the system with two-stage compression and ORC has 66.65% RTE, and the system without ORC has 62.16% RTE. For the three-stage compression configuration, the LAES system with ORC has 61.35% RTE at 190 bar. The same system without ORC has 57.51% RTE. Therefore, it can be concluded that adding the ORC increases the RTE by 6.61–7.22%.

Figure 10 also shows the net power generation by the LAES system depending on the charging pressure. Among all configurations, the most tremendous power can be generated by the 2-stage compression system with ORC. At 190 bar compression pressure, the 2-stage system with ORC has 625.5 kW net power generation, and the same system without ORC has 575 kW net power generation. Therefore, adding ORC to the system increases net power generation by 8.78%. The three-stage compression system with ORC has 494.9 kW power generation at 190 bar. The system without an ORC addition has 464.1 kW of power production under the same conditions. It can be concluded that the LAES systems with 2-stage compression and ORC have 26.6% greater power generation than the same system with 3-stage compression. The main reason behind that trend is the availability of high-temperature thermal fluid.

Figure 11 gives the influence of the discharging pressure on the round-trip efficiency and the liquid yield of the system with 2- and 3-stage compression configurations. For this case, the charging pressure is taken as constant at 190 bar. The results highlight that, for both 2-stage and 3-stage compression configurations, the round-trip efficiency is maximum at the 130 bar discharging pressure; after that, it starts to decrease. The round-trip efficiency at 130 bar discharge pressure has the greatest value of 67.65% for the 2-stage compression system with ORC, and it is followed by the same system without ORC. The three-stage compression configuration without ORC has the lowest RTE values. Figure 11 also presents the influence of the discharge pressure on the liquid yield. The liquid yield value remains almost constant between 60 and 130 bar discharging pressures at 0.85, then decreases with increasing discharge pressure.

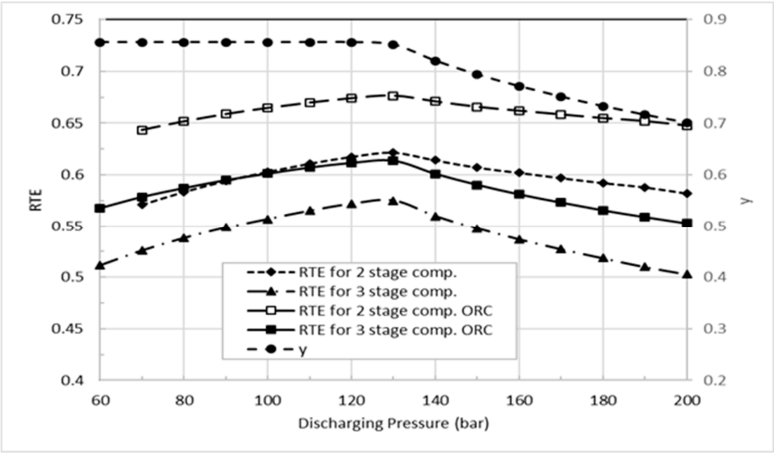


Figure 11. Variation of y and RTE with the discharging pressure for the 190 bar charging pressure.

The obtained RTE values are comparable to or higher than those reported in previous LAES studies available in the literature. Guizzi et al. [30] reported round-trip efficiencies in the range of approximately 50–60% for standalone LAES systems, while hybrid LAES configurations integrated with waste heat recovery systems generally achieved efficiencies below 65% [21,34]. The higher RTE achieved in the present study can be attributed

to the combined effects of optimized charging/discharging pressures, effective thermal energy recovery, and ORC-assisted utilization of low-grade compression heat. In particular, the proposed scalable thermal storage integration framework improves the utilization of internally recovered energy and reduces exergy destruction during the discharging process.

In Figure 12, the required amount of mass for the cold and hot storage was given for 1 MWh energy storage at 190 bar charge and 130 bar discharge pressures for the unit mass flow rate air inlet. In the literature, the mass flow rates of energy storage fluids were considered constant for all operating conditions. However, in the present work, the mass flow rate of energy storage fluids depended on the operating pressure for both the charging and the discharging processes. They are also dependent on the energy storage capacity and the system configuration. Simulation results give essential insights into thermal storage behavior for different configurations. As previously mentioned, cold and hot storage are vital for the feasible design of the LAES systems. As illustrated in Figure 12, a 3-stage compression system without ORC has the highest amount of hot thermal oil mass requirement due to the lower temperature of the hot storage fluid. A total of 14.95 tons of HTF is required for 1 MWh of energy storage capacity. The three-stage compression system with ORC has 13.87 tons of HTF requirement. The 2-stage compression system with ORC has the lowest HTF requirement, with 6.95 tons, followed by the same system without ORC, with 7.56 tons. A two-stage system with ORC has 53.51% and 49.89% lower requirements of HTF compared to the three-stage system without ORC and the three-stage system with ORC, respectively. The cold storage fluids have similar results. The LAES system with two-stage compression and ORC has the lowest requirement of methanol and propane. For 1 MWh of capacity, the system with 2-stage compression and ORC has 20% and 15.5% lower methanol and propane requirements than the 3-stage compression with ORC, respectively. Figure 12 also presents the required liquid air mass amount to achieve 1 MWh of energy discharge. Similar to the previous results, a 2-stage compression system with ORC has the lowest liquid air mass demand. To achieve the same amount of discharged energy, the LAES system with 2-stage compression and ORC has 8.14%, 18.55%, and 24.5% lower liquid air mass demand compared to the same system without ORC, a 3-stage system with ORC, and a 3-stage system without ORC, respectively. The results of the present study give essential insights regarding the thermal behavior of the hot, cold, and liquid air storage systems. High-grade waste compression heat is more valuable; therefore, it lowers the requirement for storage media. It is beneficial in terms of decreasing the storage volume. Additionally, the application of the ORC helps make use of low-grade heat and also lowers the volume of cold, hot, and liquid energy storage.

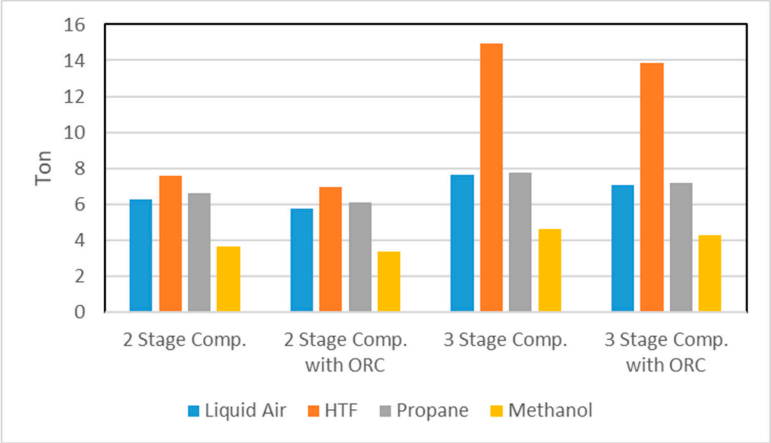


Figure 12. The cold and hot storage capacities of the 1 MWh energy storage are required for the case of 190 bar charging and 130 bar discharging pressure with the unit mass flow rate of air.

It should be noted that it is assumed that storage units are adiabatic. Since there is a time interval between the charging and discharging processes, some losses from the storage units may occur. In order to see these effects, a parametric calculation is performed. Results given in Table 5 indicate that thermal losses significantly influence system performance, particularly increasing the loss ratio, such that the 10% thermal loss results in about a 20% decrease in the RTE. Therefore, advanced insulation strategies must be applied to prevent thermal losses from the storage units.

Table 5. Comparison of the effect of the heat lost ratios from the storage units on the RTE.

Heat Loss Ratio	RTE Without ORC	Change Ratio	RTE with ORC	Change Ratio
0	62%	0	68	0
1%	61%	1.43%	67%	1.49%
5%	56%	9.45%	62%	9.3%
10%	50%	19.44%	55%	19.13%

Although the calculations in this study were performed at a constant ambient temperature of 298 K, a parametric study was performed to see the impact of ambient temperature fluctuations on the system's performance for two-stage compression with and without ORC integration. Table 6 presents the ambient temperature effect on the RTE and yield value. It is intriguing that the results show the ambient temperature does not affect the system performance significantly with respect to RTE and y values. The charging and discharging processes occur under the same ambient conditions. As the compressor work per unit liquid air mass increases with the rising ambient temperature, the recovered work per unit liquid air mass also increases with the rising ambient temperature. Therefore, the changes in RTE and y are minimal with the fluctuating air temperature.

Table 6. Ambient temperature effect on the RTE.

Ambient Temp. (K)	RTE Without ORC (%)	RTE with ORC (%)	y
278	61	67	0.84
283	61	67	0.84
288	61	67	0.84
293	62	67	0.85
298	62	68	0.85
303	62	68	0.86
308	62	67	0.86
313	62	67	0.86

4.2. Exergy Analysis

Figure 13 presents exergy flow rate ratios for the overall LAES system with two compression stages. It should be noted that the charging losses should be accounted for by considering the liquid yield value. According to the figure, 62% of the exergy input can be converted into power for the system without ORC. This also corresponds to the round-trip efficiency (RTE) of the LAES system. The overall exergy destruction rate ratio is 38%, and the discharging losses comprise the most significant amount, followed by charging losses. For the system with ORC, 68% of the exergy input can be converted into power. The exergy destruction due to the heat rejection is 8% for the system without ORC, and it is 2% for the system with ORC, respectively.

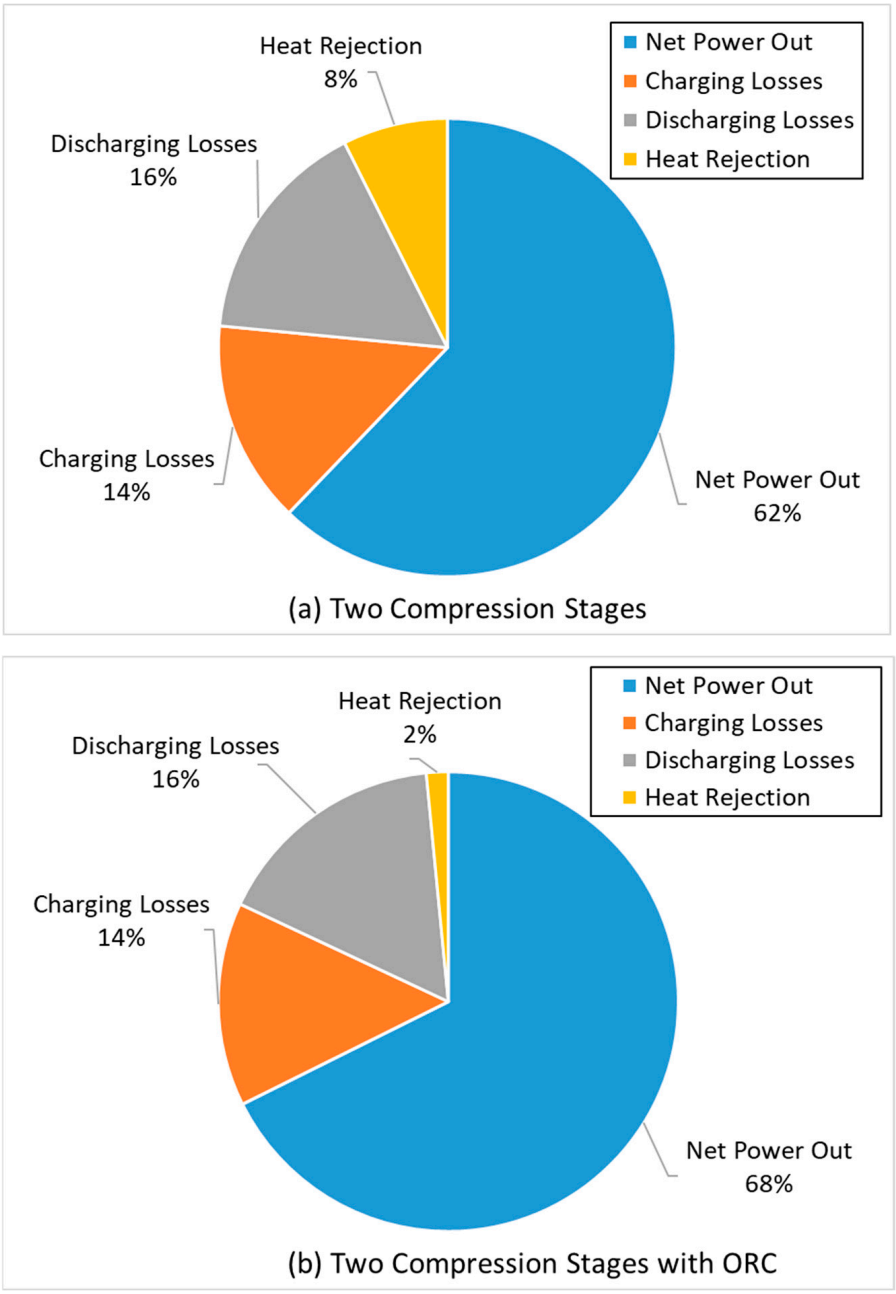


Figure 13. Exergy flow rate ratios for the overall LAES system with the two compression stages: blue: net power output; others: exergy destruction rate ratios for the two-stage compression case (**a**) and the two compression stages case with the ORC subsystem (**b**) of 190 bar charging and 130 bar discharging pressures with the unit mass flow rate of air.

Figure 14 gives the exergy flow rate ratios for the overall LAES system with three compression stages. The net power out included 58% of the overall exergy flow for the LAES system without ORC and 61% for the system with ORC, respectively. The exergy destruction rate ratio due to the heat rejection is higher (5%) for the system without ORC compared to the system with ORC inclusion (1%).

Figure 15 illustrates exergy rate outputs and exergy destruction rate ratios of the two and three-stage compression cases without ORC addition for the energy storage section. The exergy efficiency of the system for the storage section is 89% for both cases. In both cases, the most tremendous exergy destruction rate is related to the compressors.

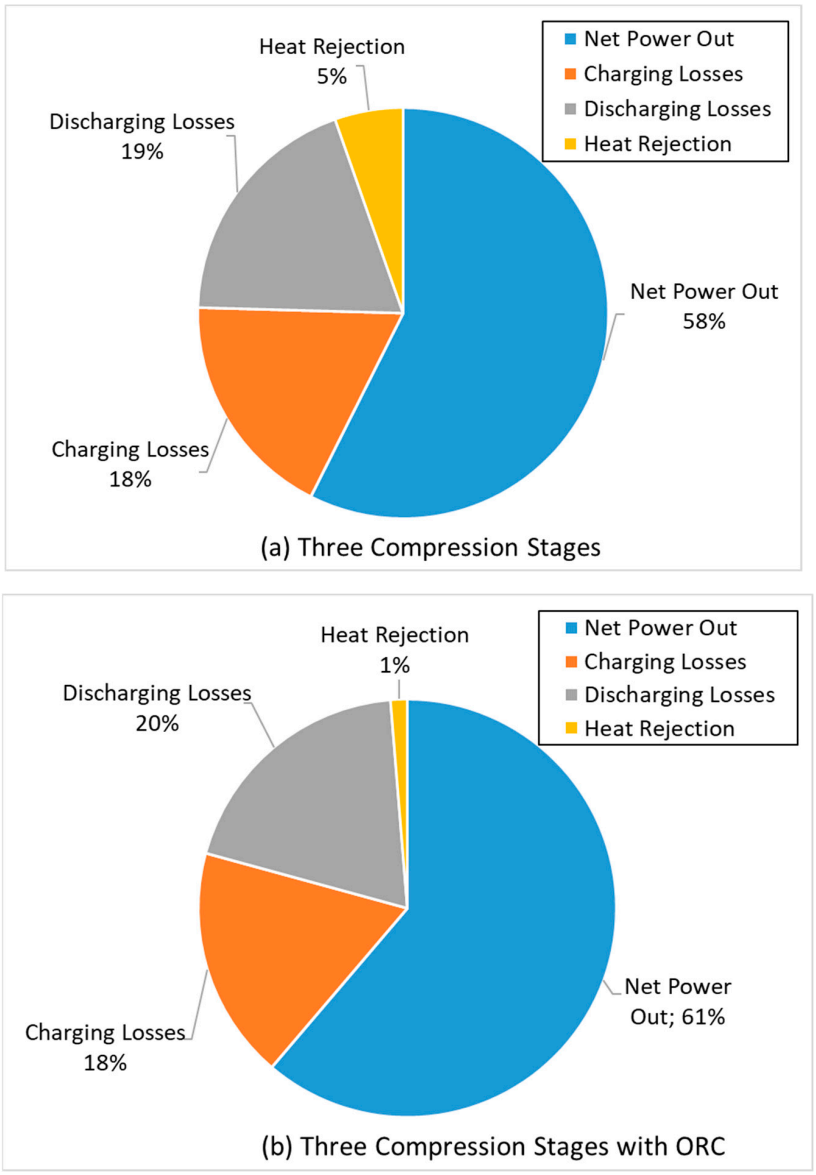


Figure 14. Exergy flow rate ratios for the overall LAES system with three compression stages: blue: net power output; others: exergy destruction rate ratios for the three-stage compression case (**a**) and the three compression stages case with the ORC subsystem (**b**) of 190 bar charging and 130 bar discharging pressures with the unit mass flow rate of air.

In Figure 16, exergy destruction rates and exergy flow ratios are given for the base case and the two-stage LAES system with ORC. The results show that the exergy efficiency of the discharging unit is 79% without ORC and 85% with ORC. Implementing the ORC subsystem into the LAES system improves the exergy efficiency of the discharging unit by 7.6%. The exergy destruction rate related to the heat rejection is 7% for the base system and 1% for the system with ORC. Therefore, it can be concluded that 6% of the destroyed exergy rate related to heat rejection was able to be gained by the ORC subsystem.

Figure 17 shows the exergy destruction rates and exergy flow ratios for three compression stages. Similar to the two-stage LAES system, the three-stage LAES system with ORC has greater exergy efficiency than the system without ORC. Implementing the ORC subsystem enhances both power output and exergy efficiency. Results also indicate that the exergy efficiency values of two-stage and three-stage LAES systems at the same conditions have the same or very close exergy efficiency values. However, the systems with two-stage compression have greater power output than those with three compression stages.

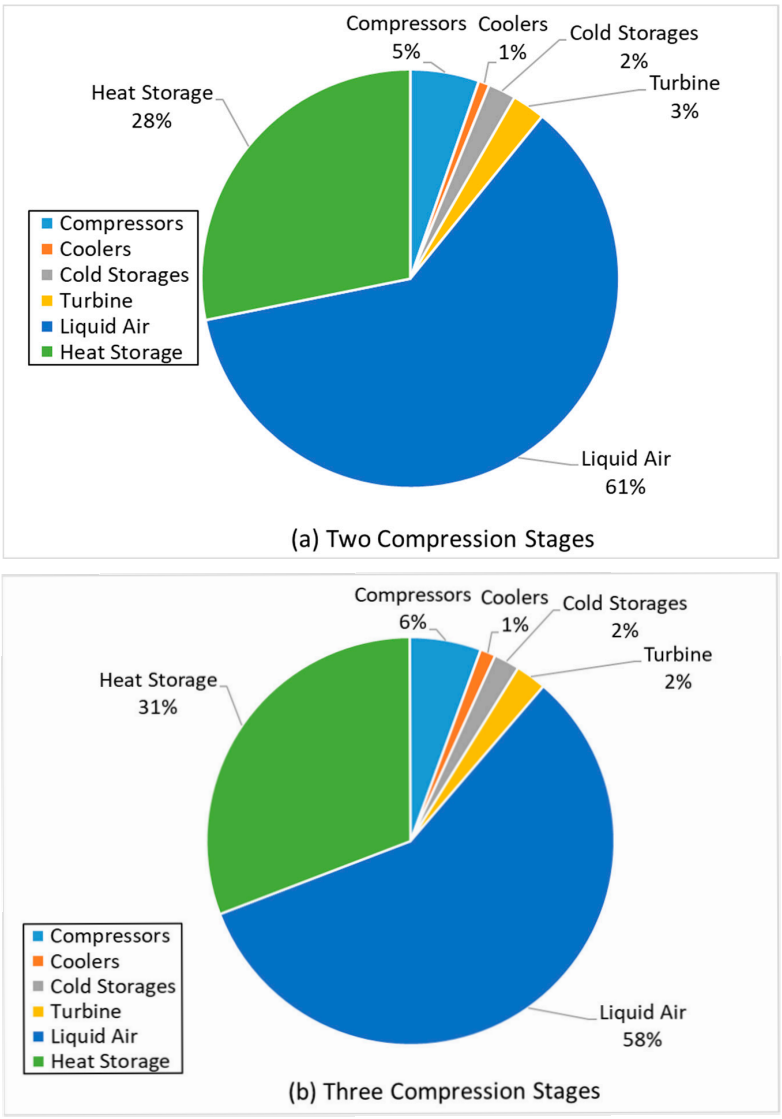


Figure 15. Exergy flow rate ratios for the energy storage section: blue and green: exergy rate outputs; others: exergy destruction rate ratios for the two-stage compression case (**a**) and the three-stage compression case (**b**) of 190 bar charging and 130 bar discharging pressures with the unit mass flow rate of air.

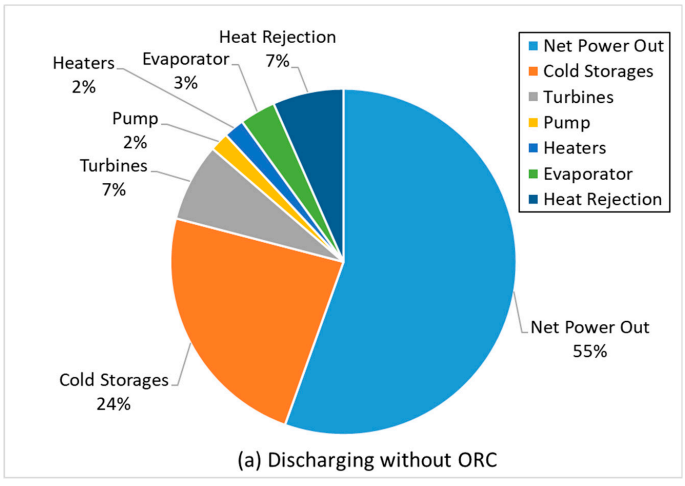


Figure 16. *Cont.*

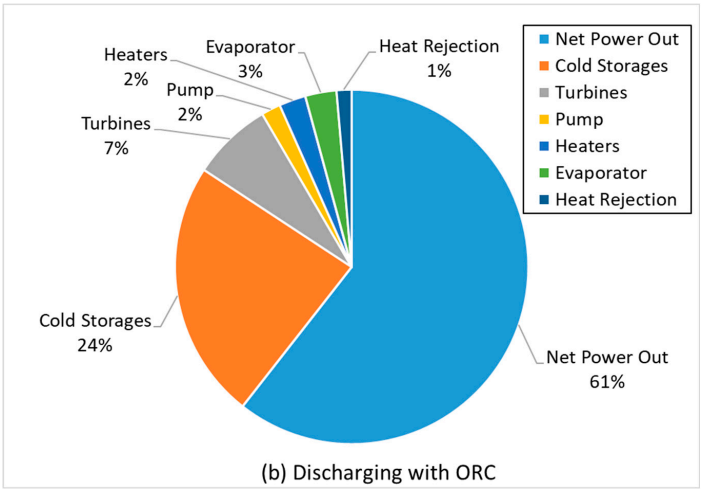


Figure 16. Exergy flow rate ratios for the energy discharging section for the two-stage compression cases: (**a**) base case, (**b**) with the ORC subsystem; blue and orange: exergy rate outputs; others: exergy destruction rate ratios for the case of 190 bar charging and 130 bar discharging pressures with the unit mass flow rate of air.

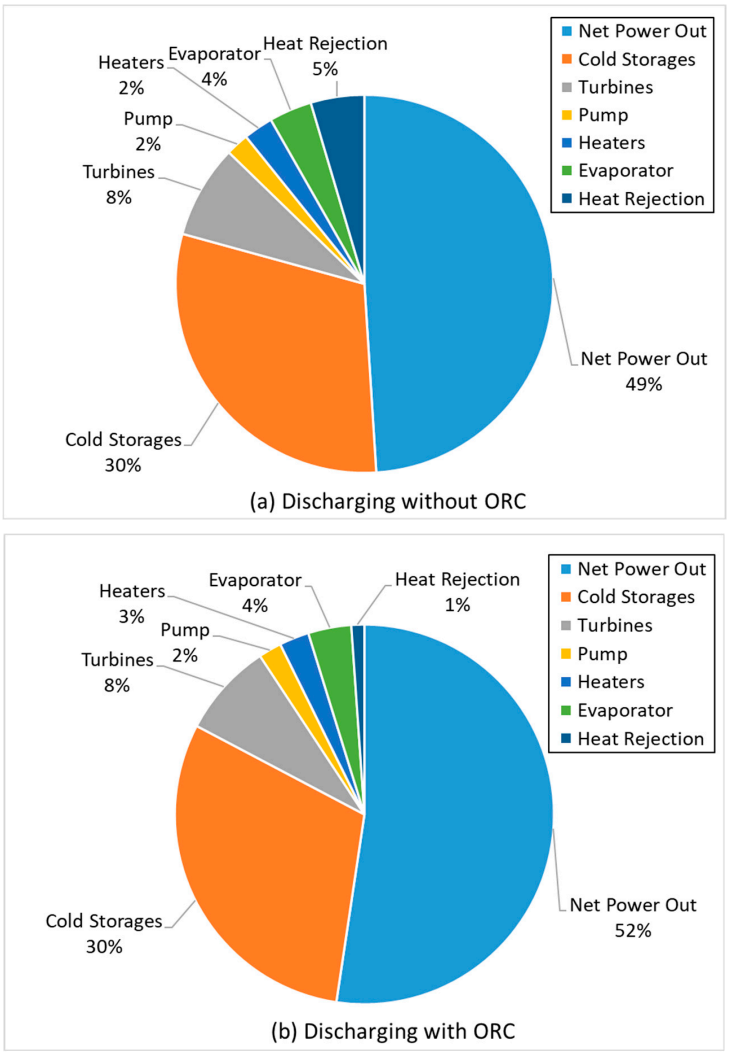


Figure 17. Exergy flow rate ratios for the energy discharging section for the three-stage compression cases: (**a**) base case, (**b**) with the ORC subsystem; blue and orange: exergy rate outputs; others: exergy destruction rate ratios for the case of 190 bar charging and 130 bar discharging pressures with the unit mass flow rate of air.

4.3. Sustainability Implications

The present results demonstrate that ORC-assisted LAES systems can contribute significantly to the development of sustainable large-scale energy storage infrastructure. Improving the round-trip efficiency of LAES systems enhances the effective utilization of renewable electricity and reduces energy losses associated with large-scale storage applications. Consequently, the proposed configuration supports the increasing penetration of intermittent renewable energy sources such as solar and wind power into modern electricity grids.

One of the important findings of this study is the reduction in thermal storage fluid requirements achieved through ORC integration. Lower storage fluid demand may reduce storage tank volume, material consumption, and auxiliary infrastructure requirements, thereby improving the overall resource efficiency and environmental sustainability of large-scale LAES deployment. In addition, the effective recovery and utilization of low-grade compression heat through the ORC subsystem contributes to enhanced energy utilization efficiency and reduced exergy destruction.

Compared with conventional large-scale energy storage technologies such as pumped hydro energy storage and compressed air energy storage, LAES systems offer important advantages, including geographical flexibility, modularity, and easier integration into urban and industrial environments. These characteristics improve the applicability of LAES technology for future decentralized and sustainable energy systems.

Furthermore, the scalable thermodynamic framework proposed in this study enables the estimation of thermal storage requirements and system performance for different energy storage capacities and operating conditions. Therefore, the proposed methodology may support future engineering design and optimization studies targeting sustainable and low-carbon power system development.

Overall, the obtained findings indicate that ORC-integrated LAES systems have strong potential for supporting renewable energy integration, improving grid flexibility, enhancing resource utilization, and contributing to sustainable low-carbon energy infrastructure.

4.4. General Discussions

The results of this study highlight the strong dependence of LAES system performance on charging and discharging pressures, the number of compression stages, and the inclusion of an ORC subsystem. Unlike many previous studies that treated thermal storage demands as constant [30,31], this work demonstrates that hot and cold storage mass flow rates vary significantly with operating conditions. This finding emphasizes the need for detailed thermal storage modeling, which has often been oversimplified in earlier works [34].

At a charging pressure of 200 bar, the liquid yield increased from 0.51 at 60 bar to 0.86, consistent with the trends reported by Borri et al. [37], who also observed that higher charging pressures enhance liquefaction efficiency. However, this study extends those insights by showing that the improved yield also reduces the required mass of hot and cold storage fluids, thereby lowering the overall system volume. For instance, the two-stage compression system with ORC reduced hot thermal fluid demand by more than 50% compared to the three-stage configuration, an aspect not previously quantified in the literature.

The round-trip efficiency (RTE) results confirm the importance of integrating auxiliary cycles. In the base case, maximum RTE was 62%, increasing to 68% with ORC integration. This 6–7% improvement is in line with the findings of Tafone et al. [47], who reported that ORC integration reduced storage costs and enhanced efficiency, Ding et al. [58], who achieved a 44.9% relative improvement by coupling LAES with solar heat and ORC, and Xin et al. [59], who performed cycle optimization in systems for recovering waste heat, and

yielded significant efficiency gains. Similarly, Chen et al. [49] demonstrated that hybrid LAES–ORC–absorption systems outperform standalone LAES in both energy and exergy terms. The present study strengthens these conclusions by showing that ORC integration not only boosts efficiency but also reduces the mass requirements of methanol and propane in cold storage by up to 20%, providing additional economic and environmental benefits.

The comparative analysis of two- and three-stage compression systems further illustrates the role of high-grade thermal energy. The two-stage configuration achieved up to 10% higher RTE than the three-stage case at equivalent pressures, due to its ability to generate higher hot storage temperatures. These results align with the observations of Nabat et al. [43], who highlighted the value of high-temperature thermal energy storage in improving exergy efficiency. The exergy analysis conducted here also confirms that compression-related irreversibility remains the dominant source of losses, as similarly reported by Hamdy et al. [60].

From a system design perspective, the results underline the significance of selecting optimal charging and discharging pressures. The maximum RTE occurred at 190 bar charging and 130 bar discharging pressures, which is consistent with the operational ranges suggested by Dzido et al. [11] and Qing et al. [20]. Beyond these limits, additional pressure increases did not yield significant performance gains, suggesting that economic considerations should dictate the choice of operating conditions.

The sensitivity analysis demonstrates that thermal losses significantly affect the overall thermodynamic performance of the proposed LAES system. As the heat loss ratio increases from 1% to 10%, the round-trip efficiency decreases progressively due to the deterioration of cold-energy preservation and reduced effectiveness of thermal recovery during the charging and discharging processes. This effect becomes more pronounced in large-scale systems where thermal storage duration is extended, and cumulative heat transfer to the surroundings increases. In particular, low-temperature cold storage is highly sensitive to environmental heat leakage because even small thermal disturbances can substantially reduce liquefaction effectiveness and increase compressor power demand during subsequent operating cycles [61]. Therefore, minimizing thermal losses is essential for maintaining high system efficiency and operational stability. From a practical engineering perspective, advanced insulation technologies such as vacuum-insulated storage tanks, multilayer cryogenic insulation systems, and low-conductivity composite materials may considerably reduce thermal degradation in industrial-scale applications [61]. Although these insulation methods increase initial capital cost, the resulting improvement in round-trip efficiency and reduction in energy losses may provide substantial long-term operational benefits. The results highlight the importance of incorporating realistic thermal-loss considerations into future large-scale LAES design and optimization studies.

Although the thermodynamic calculations in this study were primarily performed at a reference ambient temperature of 298 K, an additional sensitivity analysis was conducted to evaluate the influence of ambient temperature fluctuations under conditions of 298 K $\pm$ 15 K. The results presented in Table 6 indicate that ambient temperature variations have only a minor effect on the round-trip efficiency and liquid yield values of the proposed LAES systems. It is particularly noteworthy that the round-trip efficiency remains nearly constant within the investigated temperature range for both configurations with and without Organic Rankine Cycle integration. Similarly, only slight variations are observed in the liquid yield values. This behavior can be attributed to the fact that both the charging and discharging processes operate under identical ambient conditions. As the ambient temperature increases, the compressor work required per unit mass of liquefied air also increases. However, the recoverable expansion work during the discharging process increases correspondingly due to the higher thermodynamic state of the stored liquid

air. Consequently, these opposing effects largely compensate for each other, resulting in minimal overall variation in system performance.

Furthermore, the results demonstrate that the integrated Organic Rankine Cycle configuration maintains stable thermodynamic behavior under varying environmental conditions. This operational robustness is advantageous for practical large-scale energy storage applications, particularly in regions experiencing seasonal or climatic temperature fluctuations. The findings indicate that the proposed scalable LAES framework exhibits relatively low sensitivity to ambient temperature variations, which enhances its applicability for grid-scale renewable energy storage systems operating under different climatic conditions.

In summary, this study complements and extends the current body of knowledge by (i) explicitly linking storage fluid requirements to system pressures, (ii) demonstrating the dual benefits of ORC integration in terms of efficiency and storage volume reduction, and (iii) establishing generalized results per unit mass flow of air that are scalable across system sizes. These contributions provide practical insights for the design and deployment of LAES systems and address several gaps identified in recent reviews (Rabi et al. [10]; Liang et al. [14]; She et al. [21]). Compared with conventional large-scale energy storage technologies such as PHES and CAES, the proposed LAES–ORC system offers important sustainability advantages, including geographical independence, scalable installation capability, and improved utilization of low-grade thermal energy. Although ORC integration increases system complexity and equipment cost, the enhanced round-trip efficiency and reduced thermal storage demand may improve long-term techno-economic feasibility. Lower storage fluid requirement reduces tank volume and infrastructure demand. Furthermore, the reduction in thermal storage fluid demand achieved through ORC integration may contribute to lower material consumption and reduced infrastructure requirements for future large-scale deployment. These characteristics support the role of LAES systems in sustainable and low-carbon power-system development.

5. Conclusions

Liquid air energy storage (LAES) systems are one of the most promising energy storage systems on a grid scale. Effective use of these systems helps to increase renewable energy penetration. However, only a handful of studies focus on optimal operational configuration and internal waste heat recovery to enhance the low round-trip efficiency of these systems. In addition, the energy storage part of the previous studies is oversimplified, although it greatly influences the system's efficiency and feasibility. The present study presents a comprehensive exergy-based thermodynamic evaluation of the LAES systems with and without ORC integration. Energy storage–waste heat recovery sections, as well as the other subsystems of the LAES systems, were modeled in detail. The most significant contributions are summarized below.

- In the charging section, multi-stage compression is considered to decrease the specific energy consumption of the system. The LAES system with two- and three-stage compression was investigated. The system with two compression stages can reach higher hot storage temperatures. Therefore, the system with fewer compression stages uses high-grade thermal energy. Generally, the system with 2-stage compression has 8–10% higher round-trip efficiency values than those with 3-stage compression at the same operating conditions.
- The system's RTE and liquid yield are highly dependent on the charging and discharging pressures. Therefore, finding optimum operating conditions for the LAES systems is essential.
- Implementing ORC in the LAES systems enhances the RTE and exergy efficiency. The results showed that including ORC in the LAES systems improves the RTE by

6.61–7.22%. The exergy efficiency of the overall system with two compression stages is 62%, and it becomes 68% with the implementation of ORC. For the three compression stages, the exergy efficiency of the overall system is 58%, and it becomes 61% with the inclusion of the ORC subsystem.

- The system with 2-stage and ORC has the most remarkable power production with 625.5 kW at optimum working conditions. The same system without ORC has 8.78% lower power production. In addition, the LAES systems with 2-stage compression and ORC have 26.6% greater power generation than those with 3-stage compression.
- The influence of the various design configurations on the energy storage fluids' mass flow rates and capacity is presented for the unit mass flow rate of air. At present, the mass flow rates of energy storage fluids depend on the operating pressures for both the charging and the discharging processes. Therefore, it is possible to observe the influence of the various design conditions on the energy storage capacity.
- High-grade waste compression heat is more valuable; therefore, it lowers the requirement for storage media. It is beneficial in terms of decreasing the storage volume. Additionally, the application of the ORC helps make use of low-grade heat, and it also lowers the volume of cold, hot, and liquid energy storage.
- A two-stage system with ORC has 53.51% and 49.89% lower requirements of HTF compared to the three-stage system without ORC and with ORC, respectively. The cold storage fluids have similar results. The LAES system with two-stage compression and ORC has the lowest requirement of methanol and propane. For 1 MWh of capacity, the system with 2-stage compression and ORC has 20% and 15.5% lower methanol and propane requirements than the 3-stage compression with ORC, respectively.
- The sensitivity analyses further demonstrated that thermal losses from the storage units can substantially reduce round-trip efficiency, emphasizing the importance of advanced insulation strategies for practical large-scale implementations. In contrast, ambient temperature fluctuations within the investigated operating range exhibited only minor effects on the overall system performance due to compensating thermodynamic behavior between the charging and discharging processes. These findings indicate that the proposed LAES configurations possess favorable operational robustness under varying environmental conditions.
- Simulation results give crucial highlights about thermal storage behavior for different configurations. It is important to highlight that all calculations were made based on unit air mass flow rate. Therefore, energy storage capacity and power output are based on the unit air mass flow rate. The study results can be easily applied to systems with greater power output and energy storage capacity by increasing the air flow rate. Therefore, the results can guide future studies at various scales.
- The authors will present a future study focusing on the thermo-economic feasibility of the LAES systems and LAES systems integrated with renewable energy systems.

Author Contributions: Conceptualization, M.K.; methodology, M.K. and F.Ö.; software, M.K. and F.Ö.; validation, M.K. and F.Ö.; formal analysis, M.K. and F.Ö.; investigation, M.K. and F.Ö.; resources, M.K. and F.Ö.; data curation, M.K. and F.Ö.; writing—original draft preparation, M.K. and F.Ö.; writing—review and editing, M.K. and F.Ö.; visualization, M.K. and F.Ö.; supervision, M.K. All authors have read and agreed to the published version of the manuscript.

Funding: This research received no external funding.

Institutional Review Board Statement: Not applicable.

Informed Consent Statement: Not applicable.

Data Availability Statement: The original contributions presented in this study are included in the article. Further inquiries can be directed to the corresponding author.

Conflicts of Interest: The authors declare no conflicts of interest.

References

1. International Energy Agency. *Net Zero by 2050: A Roadmap for the Global Energy Sector*; International Energy Agency: Paris, France, 2021.
2. Huang, J.; Zhao, Y.; Song, J.; Huang, S.; Wang, K.; Rao, Z.; Zhao, Y.; Wang, L.; Wan, X.; Fei, Y.; et al. A Review of Progress in Thermo-Mechanical Energy Storage Technologies for Combined Cooling, Heating and Power Applications. *Front. Energy* **2025**, *19*, 117–143. [CrossRef]
3. Wang, W.; Yuan, B.; Sun, Q.; Wennersten, R. Application of Energy Storage in Integrated Energy Systems—A Solution to Fluctuation and Uncertainty of Renewable Energy. *J. Energy Storage* **2022**, *52*, 104812. [CrossRef]
4. Liu, Y.; Han, Y.; Peng, B.Y.; Ding, Y.; Wang, M.; Du, W.; Qian, F. Investigation of an Integrated Liquid Air Energy Storage System with Closed Brayton Cycle and Solar Power: A Multi-Objective Optimization and Comprehensive Analysis. *Fuel* **2024**, *373*, 132154. [CrossRef]
5. Jia, T.; Shuai, Y.; Wang, F.; Zhang, H.; Yang, D.; Geng, B.; Li, Q.; Wu, Q.; Xu, Y. Empowering modern power systems with thermal energy storage in China: A comprehensive review. *Renew. Sustain. Energy Rev.* **2026**, *235*, 116937. [CrossRef]
6. Zhang, Z.; Ding, T.; Zhou, Q.; Sun, Y.; Qu, M.; Zeng, Z.; Ju, Y.; Li, L.; Wang, K.; Chi, F. A Review of Technologies and Applications on Versatile Energy Storage Systems. *Renew. Sustain. Energy Rev.* **2021**, *148*, 111263. [CrossRef]
7. Liang, T.; She, X.; Li, Y.; Zhang, T.; Ding, Y. Thermo-Economic Multi-Objective Optimization of the Liquid Air Energy Storage System. *J. Energy Storage* **2024**, *84*, 110756. [CrossRef]
8. Koohi-Fayegh, S.; Rosen, M.A. A Review of Energy Storage Types, Applications and Recent Developments. *J. Energy Storage* **2020**, *27*, 101047. [CrossRef]
9. Guney, M.S.; Tepe, Y. Classification and Assessment of Energy Storage Systems. *Renew. Sustain. Energy Rev.* **2017**, *75*, 1187–1197. [CrossRef]
10. Rabi, A.M.; Radulovic, J.; Buick, J.M. Comprehensive Review of Liquid Air Energy Storage (LAES) Technologies. *Energies* **2023**, *16*, 6216. [CrossRef]
11. Dzido, A.; Krawczyk, P.; Wołowicz, M.; Badyda, K. Comparison of Advanced Air Liquefaction Systems in Liquid Air Energy Storage Applications. *Renew. Energy* **2022**, *184*, 727–739. [CrossRef]
12. Wang, C.; Bian, Y.; You, Z.; Luo, Y.; Zhang, X.; Peng, H.; Ding, Y.; She, X. Dynamic Analysis of a Novel Standalone Liquid Air Energy Storage System for Industrial Applications. *Energy Convers. Manag.* **2021**, *245*, 114537. [CrossRef]
13. Liu, Z.; Kim, D.; Gundersen, T. Optimal Recovery of Thermal Energy in Liquid Air Energy Storage. *Energy* **2022**, *240*, 122810. [CrossRef]
14. Liang, T.; Zhang, T.; Lin, X.; Alessio, T.; Legrand, M.; He, X.; Kildahl, H.; Lu, C.; Chen, H.; Romagnoli, A.; et al. Liquid Air Energy Storage Technology: A Comprehensive Review of Research, Development and Deployment. *Prog. Energy* **2023**, *5*, 012002. [CrossRef]
15. Olabi, A.G.; Wilberforce, T.; Ramadan, M.; Abdelkareem, M.A.; Alami, A.H. Compressed Air Energy Storage Systems: Components and Operating Parameters—A Review. *J. Energy Storage* **2021**, *34*, 102000. [CrossRef]
16. O'Callaghan, O.; Donnellan, P. Liquid Air Energy Storage Systems: A Review. *Renew. Sustain. Energy Rev.* **2021**, *146*, 111113. [CrossRef]
17. Larcher, D.; Tarascon, J.M. Towards Greener and More Sustainable Batteries for Electrical Energy Storage. *Nat. Chem.* **2015**, *7*, 19–29. [CrossRef]
18. Olabi, A.G.; Onumaegbu, C.; Wilberforce, T.; Ramadan, M.; Abdelkareem, M.A.; Al-Alami, A.H. Critical Review of Energy Storage Systems. *Energy* **2021**, *214*, 118987. [CrossRef]
19. Antonelli, M.; Barsali, S.; Desideri, U.; Giglioli, R.; Paganucci, F.; Pasini, G. Liquid Air Energy Storage: Potential and Challenges of Hybrid Power Plants. *Appl. Energy* **2017**, *194*, 522–529. [CrossRef]
20. He, Q.; Wang, L.; Zhou, Q.; Lu, C.; Du, D.; Liu, W. Thermodynamic Analysis and Optimization of Liquefied Air Energy Storage System. *Energy* **2019**, *173*, 162–173. [CrossRef]
21. She, X.; Wang, H.; Zhang, T.; Li, Y.; Zhao, X.; Ding, Y.; Wang, C. Liquid Air Energy Storage—A Critical Review. *Renew. Sustain. Energy Rev.* **2025**, *208*, 114986. [CrossRef]
22. Agyekum, E.B.; Odoi-Yorke, F. Liquid Air Energy Storage (LAES)—Systematic Review of Two Decades of Research and Future Perspectives. *J. Energy Storage* **2024**, *102*, 114022. [CrossRef]
23. Krawczyk, P.; Szabłowski, Ł.; Karellas, S.; Kakaras, E.; Badyda, K. Comparative Thermodynamic Analysis of Compressed Air and Liquid Air Energy Storage Systems. *Energy* **2018**, *142*, 46–54. [CrossRef]

24. Yehia, F.; Al-Haimi, A.A.N.M.; Byun, Y.; Kim, J.; Yun, Y.; Lee, G.; Yu, S.; Yang, C.; Liu, L.; Qyyum, M.A.; et al. Integration of the Single-Effect Mixed Refrigerant Cycle with Liquified Air Energy Storage and Cold Energy of LNG Regasification: Energy, Exergy, and Efficiency Prospectives. *Energy* **2024**, *306*, 132567. [CrossRef]
25. Umyshev, D.R.; Osipov, E.V.; Kibarin, A.A.; Korobkov, M.S.; Petukhov, Y.V. Analysis of Liquid Air Energy Storage System with Organic Rankine Cycle and Heat Regeneration System. *Sustainability* **2024**, *16*, 5434. [CrossRef]
26. Morgan, R.; Nelmes, S.; Gibson, E.; Brett, G. An Analysis of a Large-Scale Liquid Air Energy Storage System. *Proc. Inst. Civ. Eng.-Energy* **2015**, *168*, 135–144. [CrossRef]
27. She, X.; Zhang, T.; Cong, L.; Peng, X.; Li, C.; Luo, Y.; Ding, Y. Flexible Integration of Liquid Air Energy Storage with Liquefied Natural Gas Regasification for Power Generation Enhancement. *Appl. Energy* **2019**, *251*, 113355. [CrossRef]
28. She, X.; Peng, X.; Zhang, T.; Cong, L.; Ding, Y. Preliminary Study of Liquid Air Energy Storage Integrated with LNG Cold Recovery. *Energy Procedia* **2019**, *158*, 4903–4908. [CrossRef]
29. Zhang, J.; Wang, C. Thermodynamic and Economic Analysis of LNG-LAES and LNG-LCES Systems: A Comparative Study. *Energy* **2025**, *324*, 136047. [CrossRef]
30. Guizzi, G.L.; Manno, M.; Tolomei, L.M.; Vitali, R.M. Thermodynamic Analysis of a Liquid Air Energy Storage System. *Energy* **2015**, *93*, 1639–1647. [CrossRef]
31. Hamdy, S.; Morosuk, T.; Tsatsaronis, G. Exergetic and Economic Assessment of Integrated Cryogenic Energy Storage Systems. *Cryogenics* **2019**, *99*, 39–50. [CrossRef]
32. Hamdy, S.; Morosuk, T.; Tsatsaronis, G. Exergoeconomic Optimization of an Adiabatic Cryogenics-Based Energy Storage System. *Energy* **2019**, *183*, 812–824. [CrossRef]
33. Peng, X.; She, X.; Cong, L.; Zhang, T.; Li, C.; Li, Y.; Wang, L.; Tong, L.; Ding, Y. Thermodynamic Study on the Effect of Cold and Heat Recovery on Performance of Liquid Air Energy Storage. *Appl. Energy* **2018**, *221*, 86–99. [CrossRef]
34. Vecchi, A.; Li, Y.; Ding, Y.; Mancarella, P.; Sciacovelli, A. Liquid Air Energy Storage (LAES): A Review on Technology State-of-the-Art, Integration Pathways and Future Perspectives. *Adv. Appl. Energy* **2021**, *3*, 100047. [CrossRef]
35. Wang, C.; Cui, Q.; Dai, Z.; Zhang, X.; Xue, L.; You, Z.; She, X. Performance Analysis of Liquid Air Energy Storage with Enhanced Cold Storage Density for Combined Heating and Power Generation. *J. Energy Storage* **2022**, *46*, 103836. [CrossRef]
36. Liu, Z.; Kim, D.; Gundersen, T. Optimization and Analysis of Different Liquid Air Energy Storage Configurations. *Comput. Chem. Eng.* **2023**, *169*, 108087. [CrossRef]
37. Borri, E.; Tafone, A.; Romagnoli, A.; Comodi, G. A Review on Liquid Air Energy Storage: History, State of the Art and Recent Developments. *Renew. Sustain. Energy Rev.* **2021**, *137*, 110572. [CrossRef]
38. Kılıç, M.; Altun, A.F. Comprehensive Thermodynamic Performance Evaluation of Various Gas Liquefaction Cycles for Cryogenic Energy Storage. *Sustainability* **2023**, *15*, 16906. [CrossRef]
39. Incer-Valverde, J.; Hamdy, S.; Morosuk, T.; Tsatsaronis, G. Improvement Perspectives of Cryogenics-Based Energy Storage. *Renew. Energy* **2021**, *169*, 629–640. [CrossRef]
40. Sciacovelli, A.; Vecchi, A.; Ding, Y. Liquid Air Energy Storage (LAES) with Packed Bed Cold Thermal Storage—From Component to System Level Performance through Dynamic Modelling. *Appl. Energy* **2017**, *190*, 84–98. [CrossRef]
41. Chai, L.; Liu, J.; Wang, L.; Yue, L.; Yang, L.; Sheng, Y.; Chen, H.; Tan, C. Cryogenic Energy Storage Characteristics of a Packed Bed at Different Pressures. *Appl. Therm. Eng.* **2014**, *63*, 439–446. [CrossRef]
42. Peng, H.; Shan, X.; Yang, Y.; Ling, X. A Study on Performance of a Liquid Air Energy Storage System with Packed Bed Units. *Appl. Energy* **2018**, *211*, 126–135. [CrossRef]
43. Nabat, M.H.; Zeynalian, M.; Razmi, A.R.; Arabkoohsar, A.; Soltani, M. Energy, Exergy, and Economic Analyses of an Innovative Energy Storage System; Liquid Air Energy Storage (LAES) Combined with High-Temperature Thermal Energy Storage (HTES). *Energy Convers. Manag.* **2020**, *226*, 113486. [CrossRef]
44. Çetin, T.H.; Zhu, J.; Ekici, E.; Kanoglu, M. Thermodynamic Assessment of a Geothermal Power and Cooling Cogeneration System with Cryogenic Energy Storage. *Energy Convers. Manag.* **2022**, *260*, 115616. [CrossRef]
45. Ding, X.; Duan, L.; Li, D.; Ji, S.; Yang, L.; Zheng, N.; Zhou, Y. Dynamic Characteristics of a Novel Liquid Air Energy Storage System Coupled with Solar Heat and Waste Heat Recovery. *Renew. Energy* **2024**, *221*, 119780. [CrossRef]
46. Fan, X.; Ji, W.; Guo, L.; Gao, Z.; Chen, L.; Wang, J. Thermo-Economic Analysis of the Integrated System of Thermal Power Plant and Liquid Air Energy Storage. *J. Energy Storage* **2023**, *57*, 106233. [CrossRef]
47. Tafone, A.; Borri, E.; Comodi, G.; van den Broek, M.; Romagnoli, A. Liquid Air Energy Storage Performance Enhancement by Means of Organic Rankine Cycle and Absorption Chiller. *Appl. Energy* **2018**, *228*, 1810–1821. [CrossRef]
48. Tafone, A.; Ding, Y.; Li, Y.; Xie, C.; Romagnoli, A. Levelised Cost of Storage (LCOS) Analysis of Liquid Air Energy Storage System Integrated with Organic Rankine Cycle. *Energy* **2020**, *198*, 117275. [CrossRef]
49. Chen, Y.; Zhai, R.; Li, J.; Liu, S.; Liu, M.; Xu, Y.; Sun, C. Energy, Exergy, Economic, and Environment Evaluations of a Novel Circulating Liquid Air Energy Storage System Integrated with Organic Rankine Cycle and Absorption Refrigeration. *Process Saf. Environ. Prot.* **2025**, *195*, 106721. [CrossRef]

50. Özdemir Küçük, E.; Kılıç, M. Exergoeconomic Analysis and Multi-Objective Optimization of ORC Configurations via Taguchi-Grey Relational Methods. *Heliyon* **2023**, *9*, e15007. [CrossRef]
51. Altun, A.F.; Kılıç, M. Thermodynamic Performance Evaluation of a Geothermal ORC Power Plant. *Renew. Energy* **2020**, *148*, 261–274. [CrossRef]
52. Yağlı, H.; Koç, Y.; Kalay, H. Optimisation and Exergy Analysis of an Organic Rankine Cycle (ORC) Used as a Bottoming Cycle in a Cogeneration System Producing Steam and Power. *Sustain. Energy Technol. Assess.* **2021**, *44*, 100985. [CrossRef]
53. Méndez-Cruz, L.E.; Gutiérrez-Limón, M.Á.; Lugo-Méndez, H.; Lugo-Leyte, R.; Lopez-Arenas, T.; Sales-Cruz, M. Comparative Thermodynamic Analysis of the Performance of an Organic Rankine Cycle Using Different Working Fluids. *Energies* **2022**, *15*, 2588. [CrossRef]
54. Küçük, E.Ö.; Kilic, M. Comparative Performance Analysis of ORC—VCRC Combined Systems Based on Refrigerant Selection. *Sci. Technol. Built Environ.* **2021**, *27*, 70–84. [CrossRef]
55. Yang, J.; Sun, Z.; Yu, B.; Chen, J. Experimental comparison and optimization guidance of R1233zd(E) as a drop-in replacement to R245fa for organic Rankine cycle application. *Appl. Therm. Eng.* **2018**, *141*, 10–19. [CrossRef]
56. Eyerer, S.; Wieland, C.; Vandersickel, A.; Spliethoff, H. Experimental study of an ORC (Organic Rankine Cycle) and analysis of R1233zd-E as a drop-in replacement for R245fa for low temperature heat utilization. *Energy* **2016**, *103*, 660–671. [CrossRef]
57. Klein, S.A. Engineering Equation Solver (EES) V12. F-Chart Software: Madison, WI, USA, 2026. Available online: https://www.fchartsoftware.com/ (accessed on 17 April 2026).
58. Ding, X.; Duan, L.; Zhou, Y.; Gao, C.; Bao, Y. Energy, Exergy, and Economic Analyses of a New Liquid Air Energy Storage System Coupled with Solar Heat and Organic Rankine Cycle. *Energy Convers. Manag.* **2022**, *266*, 115828. [CrossRef]
59. Xin, Q.; Wang, J.; Mei, J.; Li, Z.; Tolj, I.; Korpebayev, D.; Bai, X.; Sun, C. Comprehensive performance analysis and optimization of the closed Brayton cycle for waste heat recovery and cooling in hydrogen aeroengines. *Energy* **2026**, *349*, 140647. [CrossRef]
60. Hamdy, S.; Moser, F.; Morosuk, T.; Tsatsaronis, G. Exergy-Based and Economic Evaluation of Liquefaction Processes for Cryogenics Energy Storage. *Energies* **2019**, *12*, 493. [CrossRef]
61. Li, J.; Fan, F.; Xu, J.; Li, H.; Mei, J.; Fei, T.; Sun, C.; Jiang, J.; Xue, R.; Yang, W.; et al. Advances in Thermal Management for Liquid Hydrogen Storage: The Lunar Perspective. *Energies* **2025**, *18*, 2220. [CrossRef]

Disclaimer/Publisher's Note: The statements, opinions and data contained in all publications are solely those of the individual author(s) and contributor(s) and not of MDPI and/or the editor(s). MDPI and/or the editor(s) disclaim responsibility for any injury to people or property resulting from any ideas, methods, instructions or products referred to in the content.